Beam Pattern Synthesis in Sensor Arrays Using Optimisation Algorithms

Author

Jonathan Daniel Gorman, BSc

The thesis is submitted to University College Dublin in part fulfilment of the requirements for the degree of ME Electronic and Computer Engineering

April 2015

School of Electrical, Electronic and Communications Engineering

Head of School: Professor Thomas Brazil

Supervisor: Professor Tony Fagan

Abstract

In this thesis optimisation algorithms are applied to a number of sensor array beam pattern synthesis problems of varying complexity. The application is primarily motivated by the expected growth of sensor networks as part of the Internet of Things (IoT) paradigm. A number of test cases are presented including a Uniform Linear Array (ULA), a ULA with an inactive element, and a 2D Wireless Sensor Network (WSN) array. The algorithms applied to the test cases include a Greedy Algorithm (GDA), a Metropolis Algorithm (MA), and a Genetic Algorithm (GA). A number of time and performance based experiments are also conducted. The results indicate that the applied optimisation algorithms offer a suitably flexible solution for optimising the beam pattern of sensor arrays, with the aim of reducing energy loss.

Acknowledgment

I would like to express my sincere gratitude to my supervisor Professor Tony Fagan for his engagement, expertise, and understanding throughout this thesis which has added significantly to my graduate experience.

I would also like to thank my family and friends who have given me unconditional support and guidance throughout my life.

Contents

I. List of Acronyms

The following table contains a list acronyms used throughout the thesis, as well as the page on which they are first used.

List of Acronyms		
Acronym	**Meaning**	**Page**
WSN	Wireless Sensor Network	8
IoT	Internet of Things	8
CB	Collaborative Beamforming	12
ULA	Uniform Linear Array	15
UCA	Uniform Circular Array	15
D-C	Dolph-Chebyshev	17
CS	Cuckoo Search	19
ABC	Artificial Bee Colony	19
SA	Simulated Annealing	19
GA	Genetic Algorithm	19
CF	Cost Function	20
UPA	Uniform Planar Array	22
NS	Node Selection	23
GDA	Greedy Algorithm	26
MA	Metropolis Algorithm	26
BR	Beam Ratio	36
EC	Elite Children	52
MC	Mutated Children	52
CC	Crossover Children	52
PSO	Particle Swarm Optimisation	82
TS	Taboo Search	82
DSC	Deep Space Communication	83

II. Table of Figures

A list of figures as they appear in this thesis is provided below, as well as the associated page number.

Chapter 1

Introduction

1.1 Motivation

The Wireless Sensor Network (WSN) is being named as one of the most important technologies of the 21st century by both research and industry (Chong & Kumar, 2003). WSNs consisting of spatially distributed autonomous sensor nodes are commonly being used to monitor and sense changes in a variety of physical parameters and conditions such as sound, temperature, pressure, etc. WSN technologies are also beginning to have a significant impact in a number of modern scenarios such as healthcare, electrical smart metering, military, environmental monitoring, and astronomy. The impact of WSNs is widely expected to increase as a result of the ubiquitous Internet of Things (IoT) paradigm (Christin, et al., 2009).

The IoT concept will see the number of everyday physical objects connected to the internet increase significantly in the coming decades, with some estimates indicating that there will be over 50 billion interconnected physical objects by 2020 (Evans, 2011). The work of Vasseur, J. &

Dunkels, A. (2011), and Alcaraz, C. et al. (2010) outline that WSNs will become increasingly integrated into the IoT, thus allowing for increased sensor communication and collaboration via the internet. Despite this, modern day issues and challenges with sensor technologies are well documented, with security (Christin, et al., 2009) and area coverage (Vu, 2009) being identified as significant problem areas. However, the issue that is primarily focused on in this thesis is energy efficiency and energy loss in a WSN.

Generally, an individual battery powered sensor is responsible for data acquisition, processing, and communication (both transmission and reception). It is found that when the energy consumption of these three functions is analysed, that the communication function consumes the most energy. Putting this into perspective, it is shown that the energy required to transmit 1 KB of data over a distance of 100 metres is approximately equivalent to a sensor carrying out 3 million instructions at a speed of 100 million instructions per second (Shebli, et al., 2007). Therefore, the communication operation is the primary consumer of the energy resources available to a sensor. Moreover, this is not aided by the fact that the battery powering a sensor is often non-rechargeable and non-replaceable, which leads to a sensor having limited electrical energy resources. These limited energy resources can cause issues with the energy autonomy of a sensor and thus, can have a detrimental effect on the overall network lifetime of the WSN which it is a part of (Feng, et al., 2009).

Furthermore, the IoT will give rise to increasingly complex WSN topologies. Such topologies include those in which sensors are located in 3D space–and–dynamic topologies where sensor locations may continually change with time. These increasingly intricate WSNs can, as will be

shown, be highly problematic with regards to energy loss and is indicated by studying the beam pattern of the WSN. Consequently, a suitably flexible solution to reducing energy consumption in WSNs, as well as adapting to changes in the topology of a WSN is required in line with the increased utilisation of WSNs as part of IoT.

1.2 Novel Contribution

The thesis attempts to introduce the first documented application of optimisation algorithms with regards to beam pattern synthesis in order to reduce energy loss in a 2D WSN. Other novel contributions include the successful optimisation of a sensor array following the loss of a significant element. The successful application of the proposed algorithms to the test cases indicates that they are sufficiently flexible to deal with the increasingly complex nature of WSNs as part of the IoT.

1.3 Thesis Layout

The thesis is composed of five distinct chapters. Following an initial background and motivation with regards to the problem, a detailed review of literature is provided in Chapter 2. This review aims to provide an in-depth overview of relevant past research, as well as its associated limitations and assumptions. It also identifies a gap in literature which this thesis attempts to assess. In Chapter 3, three test cases and three optimisation algorithms are outlined in detail. The methodology underlying the application of the algorithms to the test cases is also given. This is the succeeded by a detailed description of the acquired results in Chapter 4. Finally in Chapter 5, the thesis is concluded, the results are discussed in detail, and possible future work is identified.

Chapter 2

Literature Review

This chapter is composed entirely of a review on literature relevant to this thesis. The literature review aims to introduce necessary background knowledge, while also providing a critical evaluation of previous research undertaken on topics of interest. A number of gaps in literature are also presented which provide justification with regards to this thesis.

2.1 Collaborative Beamforming in Sensor Arrays

Extending the lifetime of battery driven sensors is a key design problem which must be solved in line with the increased usage of WSNs in modern applications. The extension of the lifetime of a sensor allows for a longer period of uninterrupted information exchange, as well as alleviating the burden of changing the battery of a sensor as frequently. It has been shown that the overhead associated with transmitting or receiving information is the most costly to the limited electrical energy resources available to a sensor (Shebli, et al., 2007) and therefore, there has been a significant effort by the research community in recent years to mitigate this problem.

In this thesis a technique known as Collaborative Beamforming (CB) is focused on in detail. CB is a transmission (or reception) technique in which multiple sensor nodes in a WSN collaborate in order to form a distributed sensor array (Figure 2.1.1). Following data acquisition by each individual sensor, the sensed data must be shared amongst all transmitting sensor nodes in the WSN. This data can now be transmitted collaboratively in the desired direction in such a way that constructive interference occurs at the receiver, located in the far-field region (Ochiai, et al., 2004). In this thesis, CB will refer to transmission only; however the theorem of reciprocity implies that the transmitted and received radiation patterns are identical.

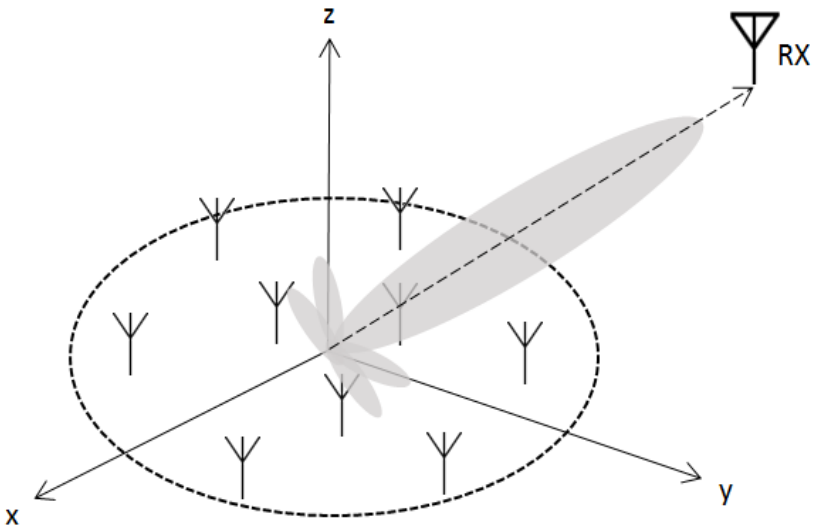

Figure 2.1.1 An illustration of CB in a 2D WSN.

Research related to CB suggests that it can be advantageous in extending the lifetime of a WSN. The network lifetime extensions come primarily as a result of an increase in transmission range, as well as improvements in the directivity of electromagnetic radiation. The improvements in directivity occur as a result of electromagnetic waves being reinforced in the direction of the receiver, as opposed to other unwanted directions. CB also helps to balance the electrical energy overhead associated with transmitting, as the energy consumed is spread over a larger

number of transmitters. CB can therefore lessen the electrical energy overhead incurred by each individual sensor as it can transmit signals at a lower power (Feng, et al., 2009).

In fact, Han, Z. & Poor, H.V. (2007) illustrated network lifetime improvements of up to 90% in uniformly spaced 2D disk networks, to as low as 10% in more complicated networks when utilising CB schemes. In this work the network lifetime was defined as the time until the first sensor node failed. Similar work presented by Tokunaga, S. (2008) analysed the power saving effect on 3 sensors with, and without, CB. The simulation results indicated that the total power consumption decreased by approximately 50% with CB, when compared to each sensor transmitting independently. The reductions in energy consumption provide evidence that CB is a feasible technique that is capable of reducing energy consumption in a WSN.

Nevertheless, it is important to state that efficient CB schemes require the proper coordination of phases amongst all transmitting sensor nodes. This coordination of phases requires an additional communication overhead, which involves energy consumption. Feng, J. et al. (2009) carried out an investigation regarding the additional energy related overheads associated with CB. The investigation attempted to determine the minimum requirements of a WSN in order for CB to be deemed worthwhile. It was found that the extent by which a sensor could reduce the power of its transmission using CB was directly proportional to the number of sensors collaborating in that transmission. Further to this, the quantity of data being transmitted by each sensor node must be shared with the network a-priori to CB. It was proven that the quantity of data being transmitted also adds significantly to the overhead associated with CB. The study proved that the number of sensors in the network, as well as the amount of data that

is to be transmitted is a critical factor in determining if CB is beneficial. This paper claimed to be the first attempting to determine the minimum network requirements for CB.

A continuation of this paper outlined how this energy consumed in a network as a result of data-sharing actually affects the overall network lifetime (Feng, et al., 2010). It was found that the energy consumed as a result of data-sharing prior to CB has negligible effects on the overall network lifetime. The effects are shown to be negligible, provided that the receiver is located significantly far away. This is as a result of the energy lost via data-sharing becoming negligible when compared with the far greater energy savings achieved via the collaborative transmission. It is also shown that the deployment radius in which the sensors are located has a direct effect on energy consumption in the WSN. Analysis showed that large deployment radiuses were found to increase the energy overhead associated with data-sharing prior to CB, as nodes must share their data with sensors which are, generally, located further away. Therefore, there are a number of constraints which must be adhered to in order to achieve adequate results from CB.

Further research, specifically related to CB in literature, focuses on schemes which operate prior to CB data-sharing. Master-slave architectures such as those detailed by Mudumbai, R. et al. (2007) and Feng, J. et al. (2010) are intended to be applied in tandem with CB. These architectures operate by splitting sensor nodes into two distinct groups – namely, sensing nodes and communicating nodes. The sensing nodes are responsible for sensing data, before transmitting it a short distance to the master node. The master node is designated as the communicating node with the greatest remaining battery life. The master node combines and compresses the data into a single packet, before multicasting the packet to each of the

transmitting nodes. The communication overhead realised as a result of data-sharing amongst nodes has therefore been reduced, as it has only been realised by approximately 50% of the network. The transmitting nodes can now collaboratively transmit the compressed data packet in the intended direction. This scheme attempts to split the load of transmitting and sensing across different sensors in an attempt to conserve energy.

Current literature is highly indicative that CB is a feasible concept by providing strong evidence that it can positively increase the lifetime of a WSN. This is despite many specific network constraints existing in order for it to be beneficial. Furthermore, it should be stated that a number of assumptions were made in the above analyses which may have influenced the final results.

2.2 Sensor Array Beam Pattern Synthesis

A sensor array is a group of sensors in which the relative phases of the transmitted signals are varied such that the resultant radiation pattern is reinforced in a desired direction and suppressed in other unwanted directions. The radiation pattern is often known as a beam pattern and is largely affected by the placement of sensors in an array. Generally, regular shaped sensor array geometries such as the Uniform Linear Array (ULA) or Uniform Circular Array (UCA) produce a more predictable beam pattern. This is in contrast to more complex geometries such as sensor arrays with elements arbitrarily located in 2D or 3D space and with no clear geometrical pattern. These more complicated geometries may not produce an acceptable beam pattern due to the diverse locations of the sensors.

A typical beam pattern is composed of a number of lobes which allow for visualisation and characterisation of where the sensor array transmits or receives power. The beam pattern typically consists of a Main Lobe (ML), a number of Side Lobes (SL), a Beam Width (BW), and a Side Lobe Level (SLL) (Figure 2.2.1). It is widely accepted that it is generally desirable to compress the BW, while also minimising the SLL as these characteristics represent radiation in unintended directions. This unwanted radiation is an energy loss and can also result in interference to other equipment (Ahmed & Vorobyov, 2009). This presents itself as a beam pattern synthesis problem where a reduction in the SLL is required in order to reduce energy loss and increase directivity of the sensor array.

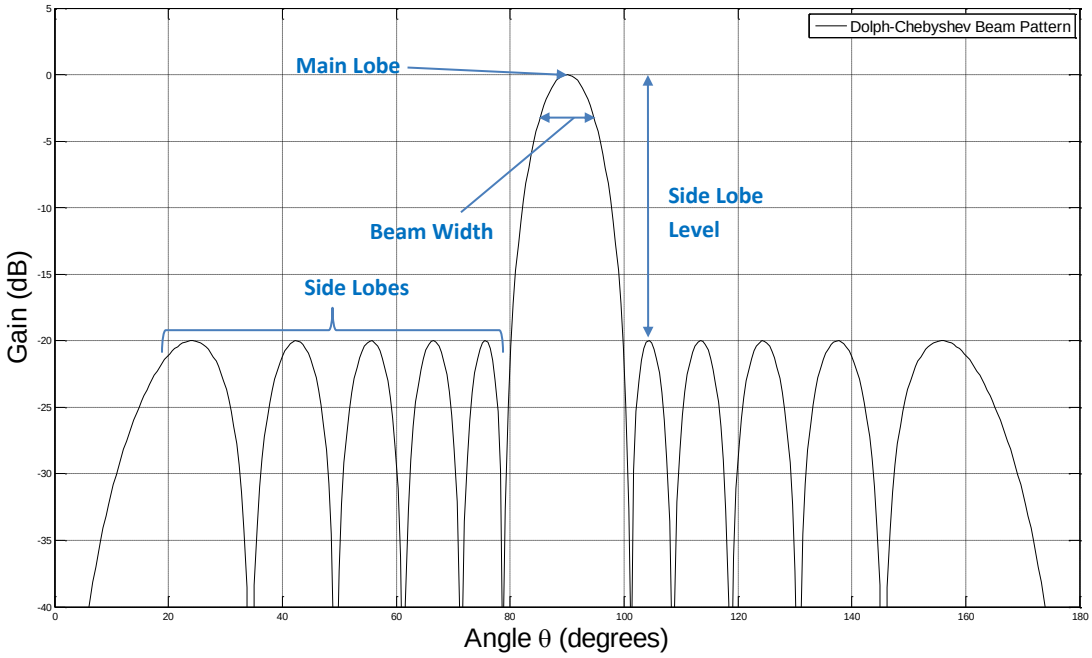

Figure 2.2.1 A plot outlining the beam characteristics of a Dolph-Chebyshev beam pattern.

The radiation beam pattern synthesis problem is well represented in literature as a result of its application in a wide variety of communications technologies. A number of synthesis approaches have been taken by the research community which have shown to be successful in reducing the SLL of an array's beam pattern. The approach taken in relation to synthesis is found

to be entirely dependent on the problem. In antenna array design procedures it is possible to change element positions according to certain cost, size or performance requirements. Certain constraints can also be applied to ensure that the resultant beam pattern meets the required specification. However, with sensor arrays it may often be the case that the element locations are not pre-located and could have positions which change with time. Therefore variables such as the currents feeding each of the elements are one of the only parameters that can be varied. It is found that the currents feeding each element of an array effects the array's beam pattern (Lakshmi & Raju, 2011).

One of the original papers on the topic of pattern synthesis was produced by Dolph, C.L. (1946) and introduced a prominent result in this field which showed the optimisation of the relationship between the BW and the SLL of a beam pattern. The proposed method provided an excitation current distribution for a ULA which resulted in a beam pattern where all of the SLs were at the same level and the corresponding BW was minimised (Figure 2.2.1). Interestingly, it is shown that in order to achieve low equi-level SLs, that a sacrifice to gain and BW is required. This provides what is often termed the minimax response and the loss in gain and BW is acceptable in many applications. This method, which is based on Chebyshev polynomials, is known in literature as the Dolph-Chebyshev (D-C) method and is widely accepted as yielding the optimum array pattern for ULAs (Zhou, et al., 1998).

The D-C methodology has been used as a basis for a variety of works in literature and has been applied to a variety of array topologies. Lau, B.K. & Leung, Y.H. (2000) used an approach based on this method, but applied it to the case of the UCA. The techniques presented were found to

be computationally efficient in achieving the minimax pattern, but were limited, as an increase in the number of nodes was found to have a negative effect on the SLL of the resulting beam pattern. This method has also been applied to non-uniformly spaced linear arrays (Zhou, et al., 1998), as well as spherical phased arrays in order to yield optimal patterns (Kumar, et al., 2009). However, methods such as the D-C method are found to be only suited to regular shaped arrays (Yanli & Yingmin, 2010) and are not entirely applicable to complex geometries, such as those which would be associated with WSNs. However, a trend is apparent in literature which aims to demonstrate that numerical methods are the most appropriate tool in providing an optimum beam pattern for an array.

2.3 A Heuristic Approach to Beam Pattern Optimisation

A variety of numerical methods have been applied to beam pattern synthesis problems in literature. These methods have included adaptive methods (DuFort, 1989), dynamic programming methods (Skolnik, et al., 1964) and conjugate gradient methods (Peters, 1989). However, as a result of the method's poor speed, robustness, and computational drawbacks in traversing the large search space associated with beam pattern synthesis; classical derivative based methods are prone to becoming trapped in one of the many local minima (Rathod & Meera, 2014). This has motivated the increased application of heuristics (including metaheuristics) to beam pattern synthesis problems. Heuristic and metaheuristic algorithms are effective in efficiently traversing large search spaces in an attempt to find a globally optimum solution, rather than a locally optimum solution (Figure 2.3.1). Metaheuristics differ from heuristics due to their entirely problem independent nature.

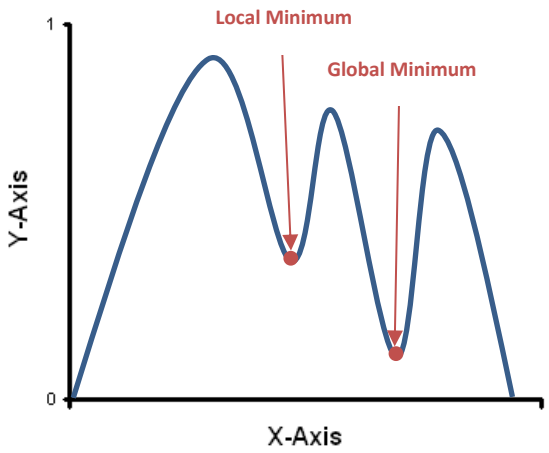

Figure 2.3.1 An illustration of a simple search space with multiple minima.

Much of the literature utilising heuristics is experimental in nature, with a variety of niche algorithms claiming novelty and efficacy in the optimisation process such as the Cuckoo Search algorithm (Khodier, 2013) and Artificial Bee Colony (ABC) algorithm. However, it is undoubted that a large proportion of literature with regards to applying optimisation algorithms for beam pattern synthesis is dedicated to the Simulated Annealing (SA) algorithm and the Genetic Algorithm (GA).

The SA algorithm is a generic probabilistic metaheuristic for global optimisation problems which attempts to find an acceptably good solution, rather than the globally optimum solution in a fixed amount of time (Rutenbar, 1989). This can, in certain cases, make SA more appropriate than exhaustive enumeration algorithms as a result of its increased computational speed. The SA algorithm is often utilised to solve real world combinatorial optimisation problems, which is the case in sensor array beam pattern synthesis (Murino, 1995). However, literature suggests that although the use of SA is widespread, it is more often applied to regularly shaped arrays. This would therefore infer that there is sufficient justification to apply the SA algorithm to more

complex cases such as the WSN, thus determining its flexibility and possible application as part of the IoT.

Current literature provides a variety of results which showcase the usefulness of SA in beam pattern synthesis problems. Vittorio, M. (1995) utilised the SA algorithm to optimise sensor positions and excitations currents of a ULA design with constraints in order to provide a specific SLL and BW via the use of a Cost Function (CF). By minimising a CF composed of variables related to the beam pattern characteristics, a specified max SL of -13.4 dB could be found. A similar study was conducted by Vittorio, M., Trucco, A. & Regazzoni, C.S. (1996) for radar and sonar signal processing where a similar SA based methodology was applied to non-uniform linear arrays. These examples of SA being used to optimise ULAs, as well as those by Farhat, N.H. & Bai, B. (1987), consistently show improvements in the resultant beam pattern characteristics. Additionally, the resultant pattern illustrated characteristics similar to those provided by the D-C optimisation method, which is substantial in providing evidence that the SA algorithm can provide an optimum solution when applied to the ULA.

Optimising wideband arrays using SA has also been explored significantly and contributes to a notable proportion of literature in regards to beam pattern synthesis. Wideband arrays are designed to have a spatial aperture greater than the length of the transmitted signals, and a typical goal is to obtain a beam pattern with a flat-top shape with suppressed SLs. This was the case in research completed by both Curletto, S. & Trucco, A. (2002) and Cardone, G. et al. who separately showed the positive benefits of the SA algorithm in order to optimise the beam pattern of wideband ULA geometries. The SA algorithm was shown to be suitable in the

synthesis procedure and produced a desired beampattern according to constraints imposed by a CF. Research in relation to the application of SA to slightly more complex array geometries has also been conducted. Ares, F. & Ferreira, J.A. (1997) computed optimal excitation currents for a 3D cylindrical array which was built using an optimised arc-array design detailed by Ares, F. et al. (1996). When the SA was applied to this specific problem it was found that a specified BW and SLL could be found via the use of SA in the synthesis procedure. Thus the application of SA to a wide range of regular array geometries exists. However, the absence of its application with regards to more complex arrays in literature leaves questions about its effectiveness in this regard.

The GA is an evolutionary inspired algorithm which, as research would suggest, is a capable method for beam pattern synthesis with the aim of reducing the SLL. The GA method was initially extended to optimisation problems by De Jong, K.A. (1975) and is characterised by being a robust, stochastic optimisation method that is modelled on the concepts of natural selection and evolution. The GA possesses the ability to locate global maxima or minima in a highly dimensional search space, and differs from other optimisation methods, including the SA algorithm, by its ability to operate on a group of trial solutions in parallel. This allows the GA to be computationally efficient, as well as being suitable for non-linear optimisation problems (Johnson & Rahmat-Samii, 1994).

There is a significant number of GA applications in literature which provide evidence that it is a highly suited to beam pattern synthesis problems. Similarly to the case of the SA algorithm, the GA is often applied to the ULA in regards to beam pattern synthesis, and literature would

suggest that it is capable of providing specified beam pattern characteristics. Work presented by Lakshmi, V.R. & Raju, G.S.N. (2011) used the D-C method to provide a current distribution to a ULA with a specified SLL and following this, the GA was used to provide further optimisation to the excitation currents. The analysis proved to be successful and resulted in max SLs in the region of -35 dB down from the ML. The application of the GA to Uniform Planar Arrays (UPA) has also been investigated by Desai, S. & Brooker, G. (2008). The simulation which was presented used a GA to synthesise the beam pattern of planar arrays used in radar systems for unmanned vehicles and aircraft. A GA was used to optimise the excitation currents of the array, but for also thinning the array, i.e., removing unnecessary elements. The performance for the thinned array was found to be comparable with the original UPA in terms of SLL, but with fewer antenna elements.

Ares-Pena, F.J. et al (1999) completed significant research in regards to the application of the GA for antenna design. A hybrid GA based array thinning method was created, which was then applied to a UPA in order to minimise the number of antenna elements, while conforming to pre-specified beam pattern characteristics. The GA was found to provide a reduction in the number of elements by 62.5% in a total of 6 iterations. The CPU time required by the GA versus an exhaustive numeration algorithm was also compared for increases in the problem complexity. It was found that as the problem complexity increased, i.e., as the number of initial elements increased, the optimisation time for the GA remained constant; whereas the optimisation time for the exhaustive enumeration algorithm increased exponentially.

An attempt to apply optimisation algorithms to more complex geometries has yet to occur in research. However, Node Selection (NS) techniques have been applied to irregular shaped sensor arrays with randomly scattered elements. NS provides an extension to optimisation algorithms by selecting only certain nodes in an array for optimisation. The nodes are often chosen such that they form a regular shaped virtual pattern such as the ULA or UCA. Notable examples of NS implementations include those showcased by Wong, W.H. et al. (2012) where a virtual circle was constructed in a random deployment of sensors in order to form a virtual UCA array topology. Following all sensing nodes successfully sharing their data with the other nodes in the virtual array, the excitation currents were then optimised using a SA algorithm. The performance was analysed and the results indicated that the selected nodes could closely mimic a UCA, provided the density of the WSNs was high enough. Other similar NS techniques which have used virtual ULAs in tandem with metaheuristics such as GA are outlined in literature (Ahmed & Vorobyov, 2009). Although few examples exist, NS presents feasible method for beam pattern synthesis in a WSN.

2.4 Antenna Array Beam Pattern Degradation

An area that is of interest to this thesis is that of element loss in an array. Elements of an array can fail during operation which can significantly degrade the quality of the resultant beam pattern. Thus, methods with the ability to re-optimise an array following the loss of an element may provide a flexible solution for optimising the beam pattern of a WSN. The loss of an array element is a common problem in areas such as ultrasound beamforming, imaging, etc., (Li, et al., 2010) and it is often found to be cheaper to apply synthesis techniques to a broken array,

than replacing the array in its entirety (Lin & Yaan Li, 2010). The loss of an element may increase the height of the SLs relative to the ML and in certain cases the level of degradation to the beam pattern is dependent on the positional prominence of the element in the array (Li, et al., 2010).

Literature presents a number of methods which attempt to compensate in an array following the loss of an element. Peters, T.J. (1990) outlined a conjugate based gradient algorithm for optimising the excitation currents in a UPA following different numbers of element failures, whereas Taşkin, A. & Gürel, C. S. (2003) utilised a GA to perform array thinning on a ULA in order to compensate for the missing elements. In the latter case, array thinning was highlighted as being the most practical method as it did not require extra phase or amplitude circuity, but instead involved simply switching off certain elements in the array. In this specific ULA case, where 5% of the array elements were broken, the GA provided an improvement in the maximum SL height of -4 dB. Thus, acceptable improvements in the beam pattern characteristics are possible using this approach.

Another notable method in literature which attempted to optimise arrays with broken elements was presented by Cui, L. & Li, Y. (2010). This research used a time delay method to linearly predict the output of an 8 element ULA in which different pairs of elements failed. This was completed by successfully varying the excitation current such that the broken element was compensated for. Although the results varied according to the pair of elements that failed, it was found that the process was capable of reconstructing the initial pattern when the least prominent first and eighth elements failed. However, maximum SL improvements of -5 dB were

also capable when the most prominent third and fourth elements failed. Thus, a method exists for reducing the cost of replacing individual array elements following an element failure, as well as minimising beam pattern degradation.

2.5 Conclusion of Literature Review

The positive effects of CB for sensor arrays in terms of reducing energy consumption are clearly presented in literature. Following CB, the resulting beam pattern is then capable of being optimised using numerical methods – particularly heuristics. The usage of SA and GA have proven effective as beam pattern synthesis techniques and are capable of reducing the SLL of an array's beam pattern. However, it was evident that the implementation of both the GA and SA is primarily to regular array geometries. Thus, the relative simplicity of the array geometries presented does not indicate that the methods are flexible enough to optimise beam patterns of sensor arrays which may have complex asymmetric geometries. Therefore with the growth of WSN technologies, as well as the associated energy problems with sensors, it is clear that there is significant justification into the undertaking of research which attempts to optimise the radiation pattern of more complex array topologies using optimisation algorithms.

Chapter 3

Applied Methodology

In this chapter, the three beam pattern synthesis test cases used in this thesis are outlined in detail, as well as any assumptions that have been made. The test cases include the ULA, the ULA with an inactive element, and the 2D WSN array. Following this, the optimisation process is detailed, and the optimisation algorithms are presented. The algorithms include the Greedy Algorithm (GDA), the Metropolis Algorithm (MA), and the GA. The simulation environment used for each of the simulations is MATLAB.

3.1 Assumptions

A number of underlying assumptions have been made with respect to each of the beam pattern synthesis test case models presented in this thesis. These assumptions are listed as follows:

- Each sensor element is assumed to be an ideal isotopically radiating element.

- All elements are assumed to be sufficiently spaced such that mutual coupling between elements does not occur.
- The single frequency assumption is valid and ensures that the frequency of electromagnetic radiation in constant throughout all experiments. The distances between elements are therefore expressed in wavelengths.
- All radiation beam patterns are observed at a distance that is far greater than the distance inter-element spacing
- Multipath fading, shadowing effects and near-field effects are ignored in all cases.
- The optimisation process takes place after any overheads associated with CB have taken place and therefore only the resultant beam pattern is of interest.
- The location of each sensor node is known to the other elements.

3.2 The Uniform Linear Array Model

The first test case model detailed is the phased ULA and represents the classic beam pattern synthesis problem outlined in literature. This model was chosen as a result of the optimum beam pattern being widely known in the form of the D-C beam pattern. The ULA model is composed of N sensor elements located in a straight line along the x-axis. The spacing between each of the elements is uniform and is given by the inter-element spacing d. The inter-element spacing d is expressed in wavelengths as a result of the single-frequency assumption. An example N element ULA is illustrated in Figure 3.2.1, where n corresponds to an individual element and θ_k (degrees) represents the angle at which the sensor array is steered relative to the x-axis. In the case of the ULA test case, only angles between 0° and 180° are analysed.

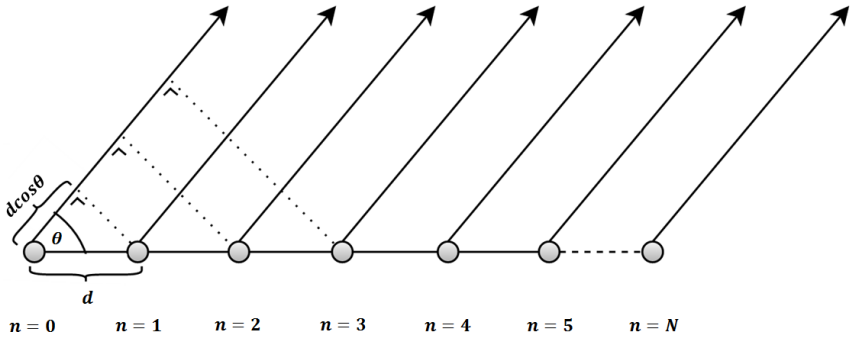

Figure 3.2.1 An Illustration of the ULA model with N isotopically radiating elements uniformly spaced in a line.

The far-field radiation pattern for a specific element n of the ULA model which is steered in a direction θ_k (degrees) is given by

$$R_{\theta_k} = I_n e^{nj(2\pi\cos(\theta_k)+\psi)} \quad \textbf{(Equation 3.2.1)}$$

where the current feeding the element is given by I_n, the number of angles is k, and ψ is the progressive phase difference. The combined far-field radiation pattern produced by the ULA for the angle θ_k can then be calculated as the sum of the individual terms, as follows:

$$R_{\theta_k} = \sum_{n=0}^{N-1} I_n e^{nj(2\pi\cos(\theta_k)+\psi)} \quad \textbf{(Equation 3.2.2)}$$

The combined far-field pattern for each element of the ULA and for all of the angles of interest is represented by the following vectorised expression:

$$\begin{bmatrix} R_{\theta_0} \\ R_{\theta_1} \\ \vdots \\ R_{\theta_k} \end{bmatrix} = \begin{bmatrix} e^{0j(2\pi\cos(\theta_0)+\psi)} & e^{1j(2\pi\cos(\theta_0)+\psi)} & \dots & e^{(N-1)j(2\pi\cos(\theta_0)+\psi)} \\ e^{0j(2\pi\cos(\theta_1)+\psi)} & e^{1j(2\pi\cos(\theta_1)+\psi)} & \dots & e^{(N-1)j(2\pi\cos(\theta_1)+\psi)} \\ \vdots & \vdots & \ddots & \vdots \\ e^{0j(2\pi\cos(\theta_k)+\psi)} & e^{1j(2\pi\cos(\theta_k)+\psi)} & \dots & e^{(N-1)j(2\pi\cos(\theta_k)+\psi)} \end{bmatrix} \begin{bmatrix} I_0 \\ I_1 \\ \vdots \\ I_{(N-1)} \end{bmatrix} \quad \textbf{(Equation 3.2.3)}$$

Equation 3.2.3 was then simplified to the following form given by

$$\vec{R} = P\vec{I} \quad \textbf{(Equation 3.2.4)}$$

where $\vec{I}$ is the complex excitation current vector feeding each of the sensor elements, P is the complex matrix of phased weights, and $\vec{R}$ is the complex vector representing the radiation beampattern.

The ULA test case outlined in this thesis has N equal to 12 elements, where each element has a uniform inter-element spacing d of 0.5 wavelengths. The excitation current vector $\vec{I}$ is initially set as unity, such that each element of the sensor array n is fed with a current as follows:

$$I_n = 1 + 0j \quad \forall \ n \in N \qquad \textbf{(Equation 3.2.5)}$$

The progressive phase difference ψ is equal to zero and the value of k is 400. Therefore there are 400 angles defined in the range of 0° to 180°, which are given by the vector $\vec{\theta}$. The absolute value of the initial radiation vector $|\vec{R}|$ was plotted against the angles of interest $\vec{\theta}$ to give the initial beam pattern (Figure 3.2.2). The symmetrical beam pattern illustrated is typical for a phased ULA, in which the SLs decrease in height according to their distance from the ML.

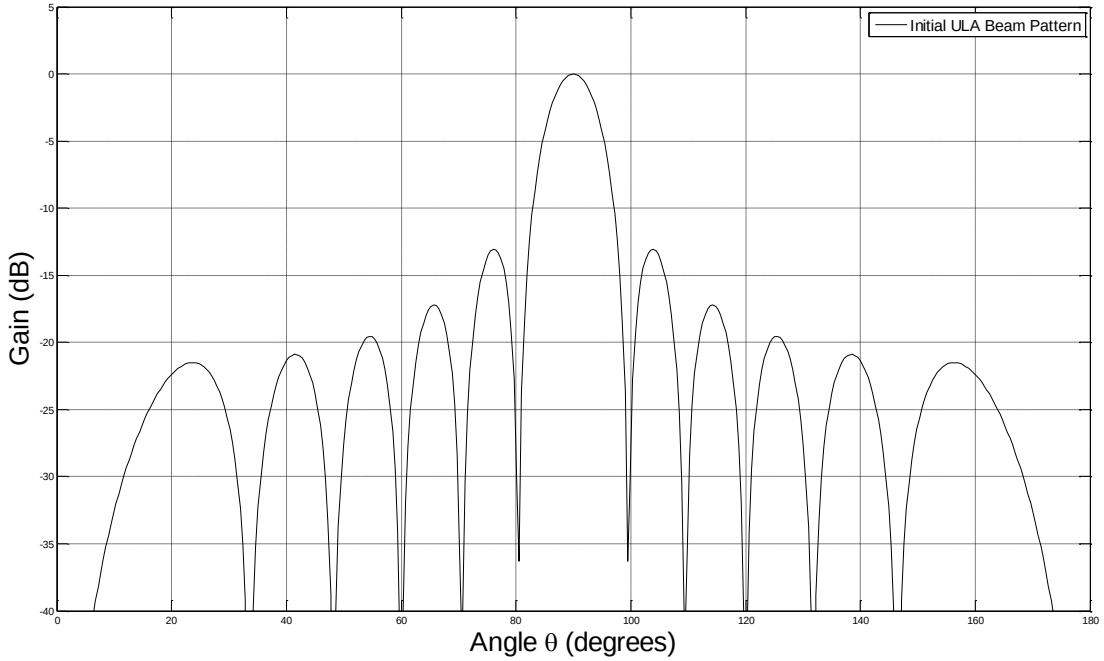

Figure 3.2.2 A plot of the initial beam pattern produced by the 12 element ULA test case.

3.3 The Uniform Linear Array with an Inactive Element Model

Element loss in an array due to failure, or otherwise, can result in performance degradation which is reflected by negative changes in the resultant beam pattern. Generally, the loss of array elements will lead to an increase in the SLL of the beam pattern, which indicates an increase in radiation in unwanted directions. Thus, the application of optimisation algorithms to this particular test case attempts to demonstrate the flexibility of the algorithms in optimising a more complex beam pattern, as well as showcasing a novel method for correcting an array following an element failure. It is envisaged that the flexible nature of the optimisation algorithms would provide WSNs with an increased degree of robustness with regards to self-healing and adaptivness following the loss or movement of key sensor elements. The ULA with an inactive element model follows directly from the ULA model described in Section 3.2. Therefore all equations outlined are still applicable to this model. However, in this case, the sixth element is inactive and so the excitation current feeding the sixth element is permanently set as follows:

$$I_6 = 0 + 0j \qquad \textbf{(Equation 3.3.1)}$$

The 12 element ULA with element 6 set as inactive has a uniform inter-element spacing *d* equal *to* 0.5 wavelengths, and a progressive phase difference ψ equal to zero. However, due to the inactivity of element number 6 the inter-element spacing between the fifth and seventh elements is equal to 1 wavelength. The angles of interest are defined by k which is equal to 400 and therefore there are 400 angles varying between 0° and 180°. The angles are given by the

vector $\vec{\theta}$, where θ_k represents the k^{th} angle. The initial beam pattern for the 12 element ULA with element 6 set as inactive is illustrated in Figure 3.3.1.

The sixth element was chosen as the inactive element due to its prominent position in the 12 element ULA. The effect of this is evident in Figure 3.3.2 where it is clear that the loss of the sixth element has a more negative impact on the SLL of the beam pattern than the loss of the third element. The loss of element 3 does not lead to major increase in the SLL, but the loss of element 6 gives rise to a SLL increase in the region of 3.2 dB.

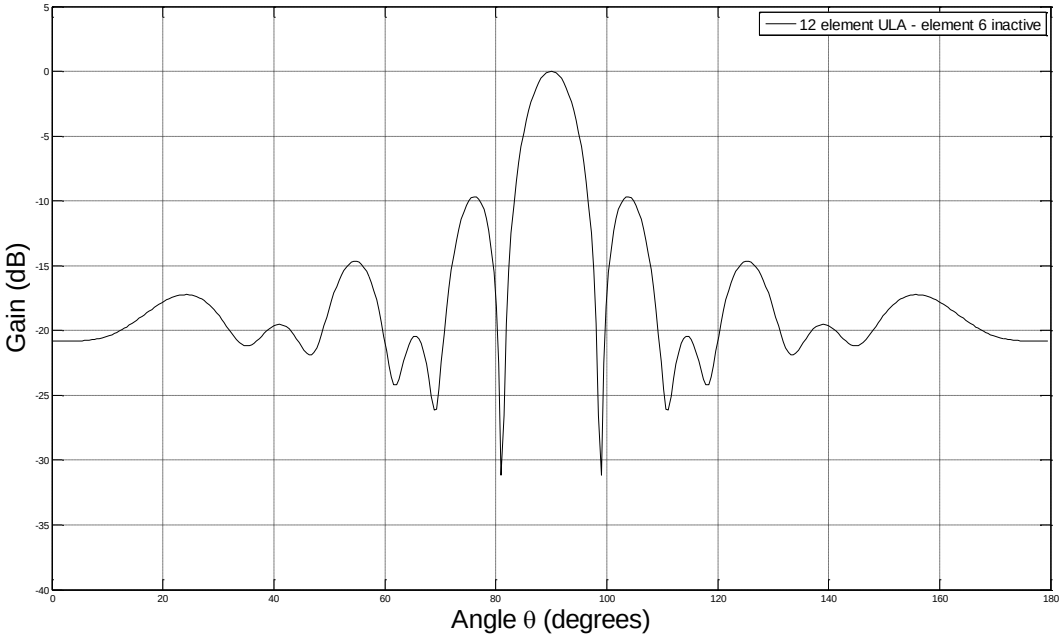

Figure 3.3.1 A plot of the initial beam pattern of the 12 element ULA with element 6 inactive.

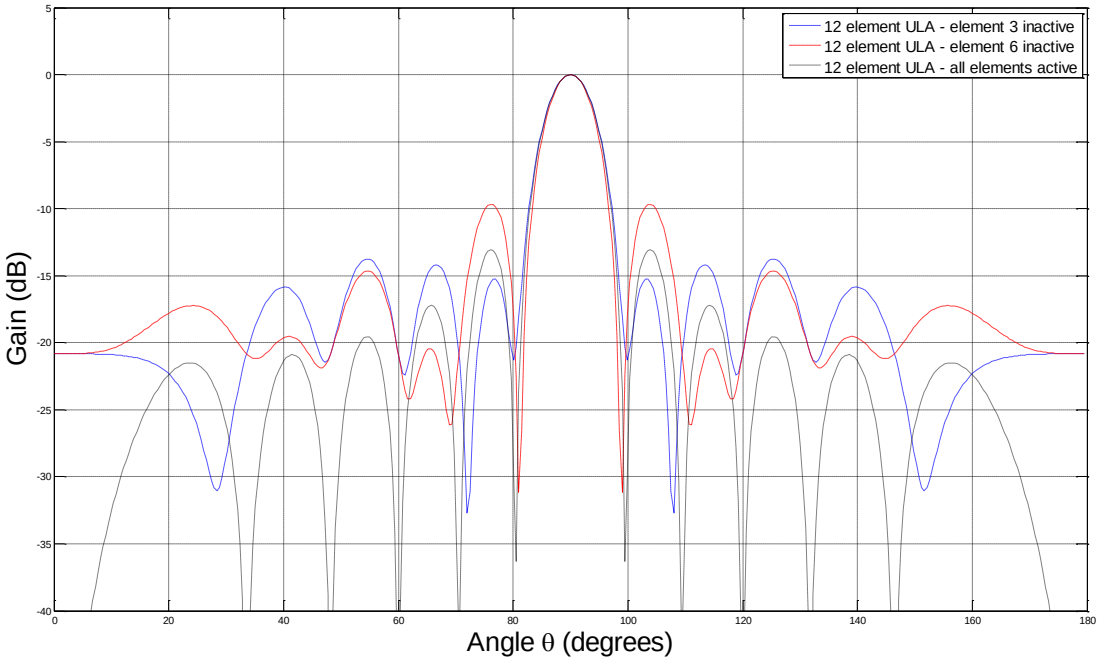

Figure 3.3.2 A plot comparing the beam patterns of a 12 element ULA with different pairs of elements set as inactive.

3.4 The 2D Wireless Sensor Network Array Model

The 2D WSN array model consists of N isotopically radiating sensor elements randomly distributed in a 2D circular network of radius d (wavelengths). The model attempts to replicate a WSN of collaborating sensor elements in a 2-dimensional plane. The elements are scattered according to a Gaussian distribution such that the suitability and flexibility of the algorithms can be thoroughly tested. The random deployment of sensors in the WSN array leads to a large variations in the resulting beam patterns. The sensor array model operates under the assumptions outlined in Section 3.1.

A sensor element n is represented in terms of its polar coordinates r_n (radial) and ϕ_n (angular) in the WSN. The far-field pattern produced by a single sensor element in the direction of θ_k is the phasor given by

$$R_{\theta_k} = I_n e^{-j2\pi \mathrm{r_n}\cos(\theta_k - \phi_n)} \quad \textbf{(Equation 3.4.1)}$$

where I_n represents the excitation current feeding the particular sensor element n. The combined far-field pattern for all N sensor elements in the network and steered at an angle θ_k is therefore given as follows:

$$R_{\theta_k} = \sum_{n=0}^{N-1} I_n e^{-j2\pi r_n \cos(\theta_k - \phi_n)} \quad \textbf{(Equation 3.4.2)}$$

The combined far-field radiation pattern for each sensor element in the WSN and for all of the angles of interest is represented by the following expression:

$$\begin{bmatrix} R_{\theta_0} \\ R_{\theta_1} \\ \vdots \\ R_{\theta_k} \end{bmatrix} = \begin{bmatrix} e^{-j2\pi \mathrm{r_0}\cos(\theta_0 - \phi_0)} & e^{-j2\pi \mathrm{r_1}\cos(\theta_0 - \phi_1)} & \dots & e^{-j2\pi \mathrm{r_{(N-1)}}\cos(\theta_0 - \phi_{(N-1)})} \\ e^{-j2\pi \mathrm{r_0}\cos(\theta_1 - \phi_0)} & e^{-j2\pi \mathrm{r_1}\cos(\theta_1 - \phi_1)} & \dots & e^{-j2\pi \mathrm{r_{(N-1)}}\cos(\theta_1 - \phi_{(N-1)})} \\ \vdots & \vdots & \ddots & \vdots \\ e^{-j2\pi \mathrm{r_0}\cos(\theta_k - \phi_0)} & e^{-j2\pi \mathrm{r_1}\cos(\theta_k - \phi_1)} & \dots & e^{-j2\pi \mathrm{r_{(N-1)}}\cos(\theta_k - \phi_{(N-1)})} \end{bmatrix} \begin{bmatrix} I_0 \\ I_1 \\ \vdots \\ I_{(N-1)} \end{bmatrix}$$

(Equation 3.4.3)

This can then be simplified to an expression where $\vec{R}$ is the complex vector representing the radiation beampattern, P is the complex matrix of phased weights and $\vec{I}$ is the complex excitation current vector feeding each of the sensor elements. This is then written as follows:

$$\vec{R} = P\vec{I} \quad \textbf{(Equation 3.4.4)}$$

The test case presented has N equal to 32 randomly scattered sensor elements in a circular network of radius *d* equal to 2 wavelengths, and where a mock receiver is located at 180° to the x-axis. The aim of the mock receiver is to indicate the direction that the beam is steered and has no bearing on the simulation. The number of angles k used was 400, such that the vector of angles is given by $\vec{\theta}$, where the k^{th} angle is represented by θ_k.

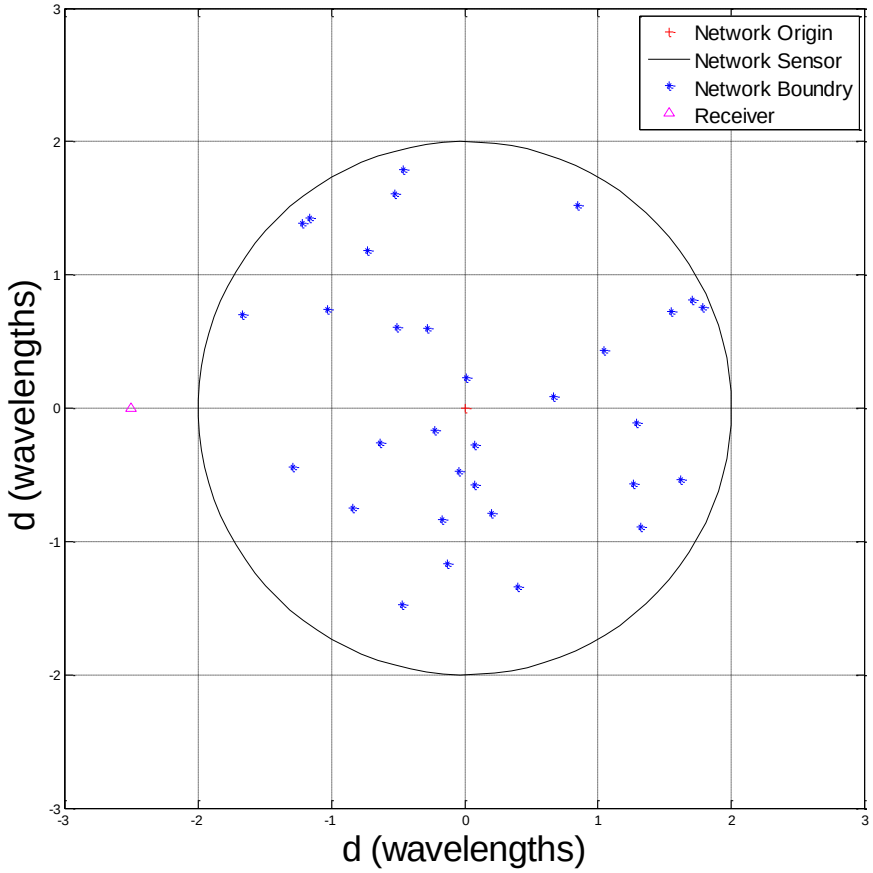

Figure 3.4.1 A randomly generated 32 element WSN.

The initial excitation current vector was created in order to steer the array was steered towards 180°. This is completed by setting the current feeding each of the elements n equal to the conjugate of the phased weight corresponding to that element n, for the angle k which points in the direction of 180°. this is denoted as θ_{180° and given for an individual element n as follows:

$$\overrightarrow{I_n} = \overline{e^{-J2\pi \mathrm{r}_0 \cos(\theta_{180^\circ} - \phi_0)}} \qquad \textbf{(Equation 3.4.5)}$$

The absolute value of the complex radiation beam pattern matrix $\left|\vec{R}\right|$ was plotted against the corresponding angles given by $\vec{\theta}$ to provide the initial beampattern (Figure 3.4.2). The beam pattern is highly asymmetrical in nature and has a maximum SL is in the region of -8 dB down from the ML. The maximum SL height is not dissimilar to the initial beam pattern of the ULA and

ULA with an inactive element beam patterns; however, it is clear that there are a number of additional distinct SLs of similar height. These SLs in the initial pattern of the WSN array indicate that there is significant energy loss associated with the geometrical structure of the sensor array. Furthermore, the random nature of the sensors ensures that the level of the SLs is entirely arbitrary in this model. Therefore this model offers the largest challenge posed to the optimisation algorithms outlined in this thesis. The 2D WSN array model will correctly distinguish whether the proposed algorithms are flexible enough to adapt to the random nature of a beam pattern produced by a WSN array.

However, it should be noted that for comparison purposes, the random number generator provided by MATLAB is initially seeded in order to produce an identical random element distribution in each WSN array simulation as given in Figure 3.4.1. This is in order to fairly compare each of the algorithms applied to the WSN array test case.

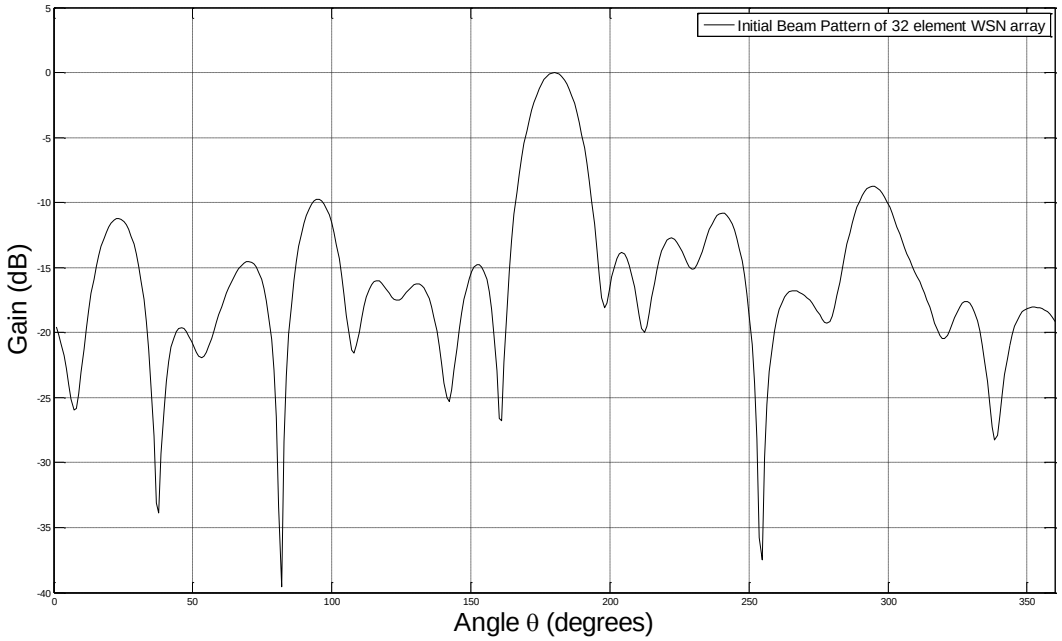

Figure 3.4.2 A plot of the initial beam pattern produced by the 32 element WSN array

.

3.5 The Optimisation Process

The process underlying each of the three optimisation algorithms is similar in certain respects. The beam pattern synthesis problem is presented as a minimisation problem in which the algorithms are required to minimise the value of a CF. It is possible to represent a beam pattern in terms of a CF which aims constrain the beam pattern synthesis procedure and thus enforces specific beam pattern characteristics. The CF in all test cases is defined as the ratio of the maximum SL to the ML of the beam pattern, given by value known as the Beam Ratio (BR) as follows:

$$BR = \frac{SL_{max}}{ML} = CF \qquad \textbf{(Equation 3.5.1)}$$

The BR is a dimensionless quantity, were a low value corresponds to a high SLL, which represents a low maximum SL and a reduction in the radiation being transmitted in unintended directions by the sensor array. The initial value of the CF in each of the test cases is set according to the initial beam characteristics, as shown in Figures 3.2.2, 3.3.1, and 3.4.2 respectively. The initial excitation current vector, which is termed $\vec{I}_{initial}$, determines the initial beam pattern, and therefore determines the corresponding initial CF value. The variation of the initial excitation current vector $\vec{I}_{initial}$ therefore results in changes in the value of the CF. The globally optimum solution for a given test case is therefore the optimum current excitation vector $\vec{I}_{optimum}$ which minimises the value of the CF such that the maximum SL approaches zero. However, there is no way of determining the optimum excitation vector $\vec{I}_{optimum}$ as a

result of the exhaustively large search space. Each of the algorithms must therefore attempt to find $\vec{I}_{best}$, which is an approximate to $\vec{I}_{optimum}$.

An iterative process is performed, whereby at each iteration the best excitation current vector $\vec{I}_{best}$ feeding the elements of the sensor array is varied according to the algorithm used. Following this, the resultant beam pattern characteristics are computed and the CF is re-evaluated (Figure 3.5.1). Each of the optimisation algorithms presented differ primarily with regards to the variation of the best excitation current vector $\vec{I}_{best}$, and their subsequent actions according to changes in the CF.

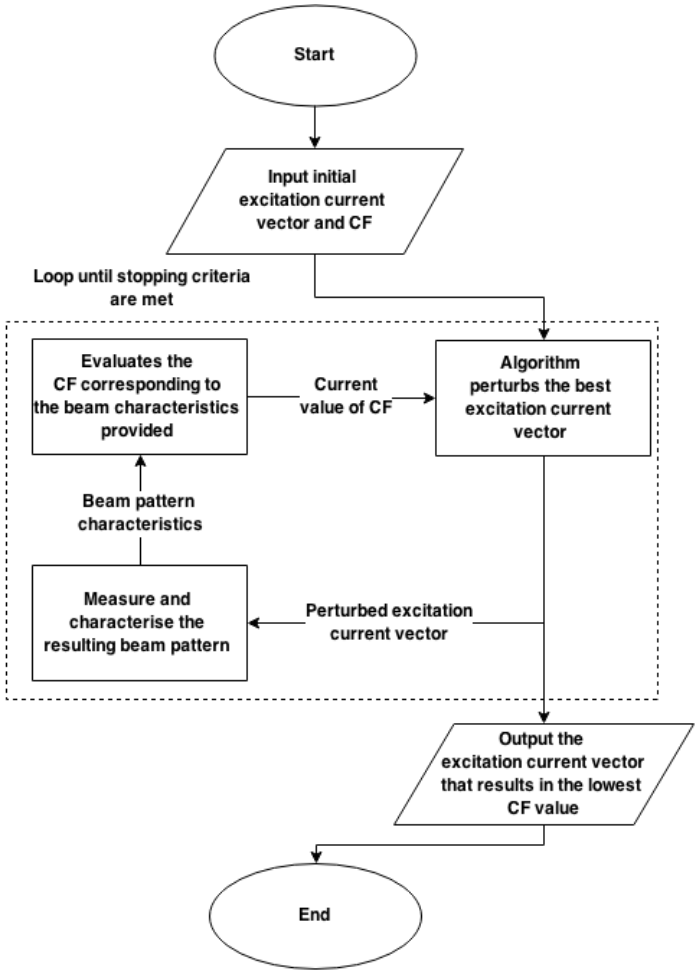

Figure 3.5.1 A flowchart of the optimisation process undertaken by the algorithms.

In each of the test cases, the beam pattern is composed of k equal to 400 individual angles. The optimisation process characterises each beam pattern according to the height of its ML, max SL, SLL and BR. However, the algorithms may cause changes in the excitation current vector which can dramatically change the resulting beam pattern. The beam pattern may be affected in such a way that issues with its characterisation occur. These issues include major fluctuations in the current excitation vector which can see minor SLs become highly prominent, i.e., higher than the ML. The search space is therefore segmented in order to ensure that certain beam characteristics can only occur in specified regions of the search space. The segmentation procedure also allows for the introduction of two transition regions or 'do not care' regions which mark the intervals where the ML transitions into the adjacent SL. The segmentation of the k angle beam pattern, where k is equal to 400 is outlined in Table 3.5.1.

Table 3.5.1 Segmentation of Beam Pattern Characteristics and Corresponding Angles

Angles k	**Beam Pattern Characteristic**
0 - 175	Left Maximum Side Lobe*
175 - 190	Left Transition Region
190 – 210	Main Lobe
210 – 225	Right Transition Region
225 - 400	Right Maximum Side Lobe*

***The maximum SL is chosen as the larger of the left and right peak side lobes.**

Each of the optimisation algorithms discussed in this thesis will be applied to the three test cases in four separate experiments. This is in order to investigate a variety of constraints and stopping criteria which may produce different results from a particular algorithm. The algorithms will be applied to each of the test cases with, and without, a constraint on the

excitation current vector $\vec{I}_{best}$. In the former case, the excitation current vector feeding a specific sensor element n will be bounded by the following condition:

$$(-5 - 5j) \leq I_n \leq (5 + 5j) \quad \textbf{(Equation 3.5.2)}$$

The bounded condition, when applicable, is applied to the currents feeding all sensor elements $n \in N$. The bounded case is considered as it aims to determine the effectiveness of an algorithm in providing a realistic excitation current vector which optimises the beam pattern of the array. In practice it is found that array element currents which are too large, too small, or where there is a large difference between adjacent currents may not be implementable. The algorithms will therefore be applied to each of the test cases with bounded and unbounded excitation vectors. In order to quantify the relative size and assign a strictly positive size of an optimised excitation current vector $\vec{I}$, the 2D Euclidian norm will be used. The current excitation vector norm $\|\vec{I}\|$ is computed for comparison purposes between the relative sizes of excitation current vectors produced by each of the algorithms.

As well as the bounded current criteria, two distinct stopping criteria are also tested. The stopping criteria used in conjunction with each of the algorithms are based on time and performance measures. Each of the stopping criteria will be applied separately to the bounded and unbounded excitation current cases. In the time based experiments, each algorithm will be allowed to operate for 1500 ± 0.02% seconds (25 ± 0.02% minutes). The time based criteria aims to distinguish which of the three algorithms applied can provide the lowest CF value in the given time limit. The error margin on the time limit is to allow sufficient time for an algorithm to cease operation following the time limit being reached.

The aim of the performance based tests is to determine which of the three algorithms is the most effective in reaching a target CF value in the shortest amount of time. The algorithms effectiveness is measured by the speed in which it provides a solution equal to the target CF value. The target CF value differs according to the complexity of each of the test cases. The target CF value is initially determined according to the algorithm that produced the highest (i.e. worst) CF value in the time based experiments. The target CF values for each of the test cases are detailed in Table 3.5.2.

Table 3.5.2 Target CF Values for All Performance Based Tests

Test Case	Target CF
ULA	0.075
ULA with Inactive Element	0.180
WSN Array	0.200

Due to the stochastic nature of the algorithms presented, it is possible that results may vary significantly for multiple simulations of the same experiment. Therefore, each algorithm is applied 15 times to each test case, and provides 15 samples in each experiment. In the time based experiments, the sample which yielded the lowest CF value is chosen. Similarly in the case of the performance based experiments, the sample which yielded the target CF in the shortest amount of time was chosen.

The systems parameters on which each of the simulations was conducted is given in table 3.5.3 below. This is order to ensure that accurate reconstruction of the experiments is possible.

Table 3.5.3 Simulation Environment System Parameters

System Parameter	Parameter Value
MATLAB Version	R2013a
Processor	Intel Core i3-3220
CPU Clock Rate	3.30 GHz
Operating System	Windows 32-bit
Memory (RAM)	4 GB

3.6 The Greedy Algorithm

The GDA is a stochastic search heuristic that employs a scheme by which the locally optimal choice is made at each stage of the optimisation process. The GDA is often termed as 'irreversible' in nature as a result of the algorithm not reconsidering a decision once it is made. As a result of this, the GDA is highly dependent on its initial conditions and generally the algorithm is characterised by not producing a globally optimum result. This is due to the algorithm being unable to traverse a large search space as a result of its 'greedy' nature in searching for a locally optimum solution.

A simple example demonstrating this is provided below in Figure 3.6.1 where the GDA is attempting to calculate the largest sum possible. With this goal in mind, at the first decision point the GDA makes the locally optimal choice, therefore choosing 5 instead of 3. However, the GDA has overlooked the value of 99 which would have resulted in the largest possible sum being found. Due to the irreversible nature of the GDA, the optimum solution cannot be found.

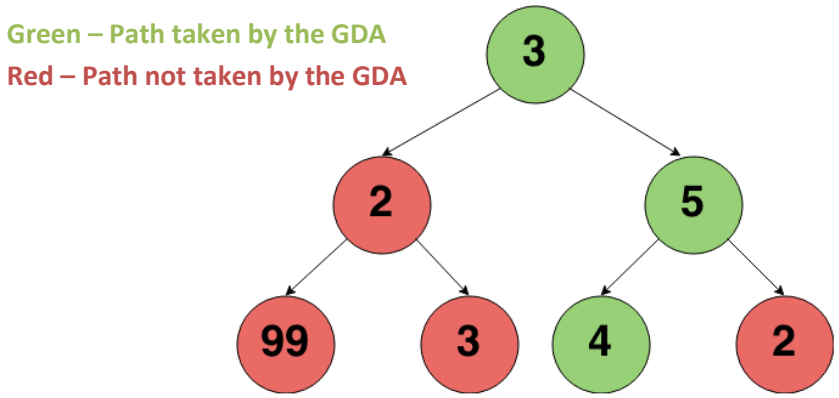

Figure 3.6.1 A demonstration of the GDA decision making process.

Given the initial excitation current vector $\vec{I}_{initial}$ and the corresponding initial value of the CF, the GDA stores the initial excitation current vector as $\vec{I}_{best}$. Following this, the GDA attempts to find the optimum excitation current vector $\vec{I}_{optimum}$ such that the CF is minimised. The GDA attempts to minimise the CF by adding complex random Gaussian perturbation vectors to the best excitation current vector $\vec{I}_{best}$ at each iteration. A perturbation vector is given by $\vec{\kappa}$, where its addition to $\vec{I}_{best}$ generates a new excitation current vector $\vec{I}_{perturbed}$. This expression is given as follows:

$$\vec{I}_{perturbed} = \vec{I}_{best} + \vec{\kappa} \qquad \textbf{(Equation 3.6.1)}$$

The perturbed excitation current vector $\vec{I}_{perturbed}$ is applied to the sensor array elements, following which the resulting beam pattern is characterised and the corresponding perturbed CF is established. At this point the GDA compares the values of the best CF and perturbed CF. If the perturbed CF is lower than the best CF, the perturbed parameters overwrite the best parameters. Conversely, if the addition of the perturbation vector $\vec{\kappa}$ to the best excitation current vector $\vec{I}_{best}$ does not yield a reduction in the CF, the resulting perturbed parameters are discarded.

The algorithm ensures that the best excitation current vector $\vec{I}_{best}$ can progress towards an $\vec{I}_{optimum}$, by the continued addition of perturbation vectors $\vec{\kappa}$. However, it is found that reducing the magnitude of the $\vec{\kappa}$ vector over time can result in the GDA to producing a lower CF. The lower CF is as a result of the algorithm being capable of traversing a larger search space, which is revealed by the smaller perturbations. Thus a scaling factor σ is utilised by the GDA in order to control the magnitude of the perturbation vector $\vec{\kappa}$. Therefore the underlying formula underlying the GDA can be expressed by

$$\vec{I}_{perturbed} = \vec{I}_{best} + \vec{\kappa}\sigma \qquad \textbf{(Equation 3.6.2)}$$

where the scaling factor σ used by the GDA is reduced from 0.5 to 0.01. The rate of decrease in σ is determined by the by the stopping criteria of the algorithm, namely a maximum time limit or a maximum iteration count. An example plot of the value of the scaling value $\sigma = \{0.5, 0.4, 0.25, 0.2, 0.1, 0.05, 0.01, 0.005\}$ for 210,000 iterations is given below.

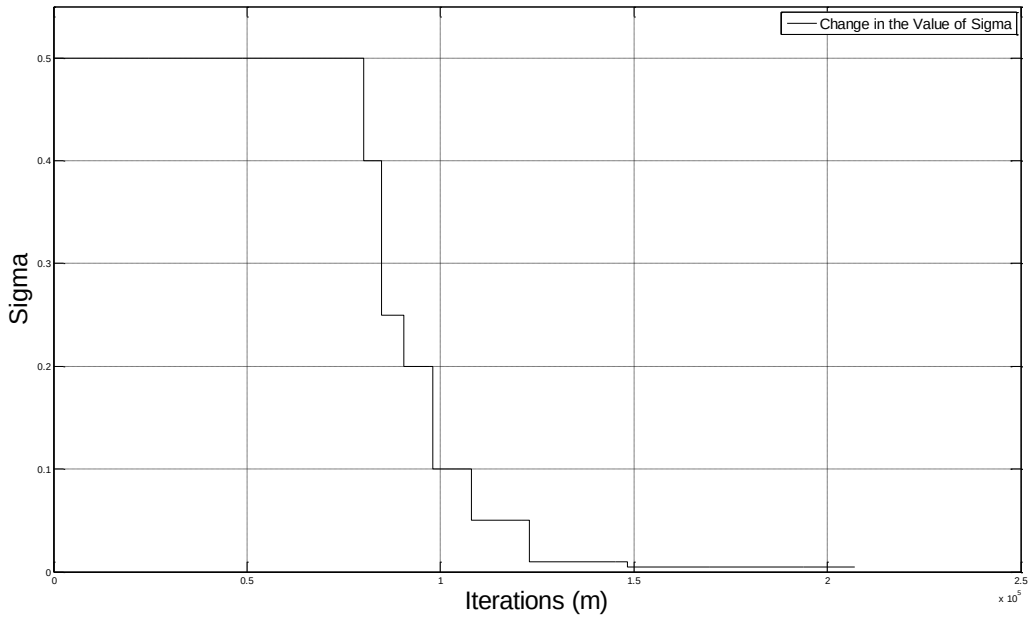

Figure 3.6.2 A plot outlining the change in the σ value versus the number of iterations.

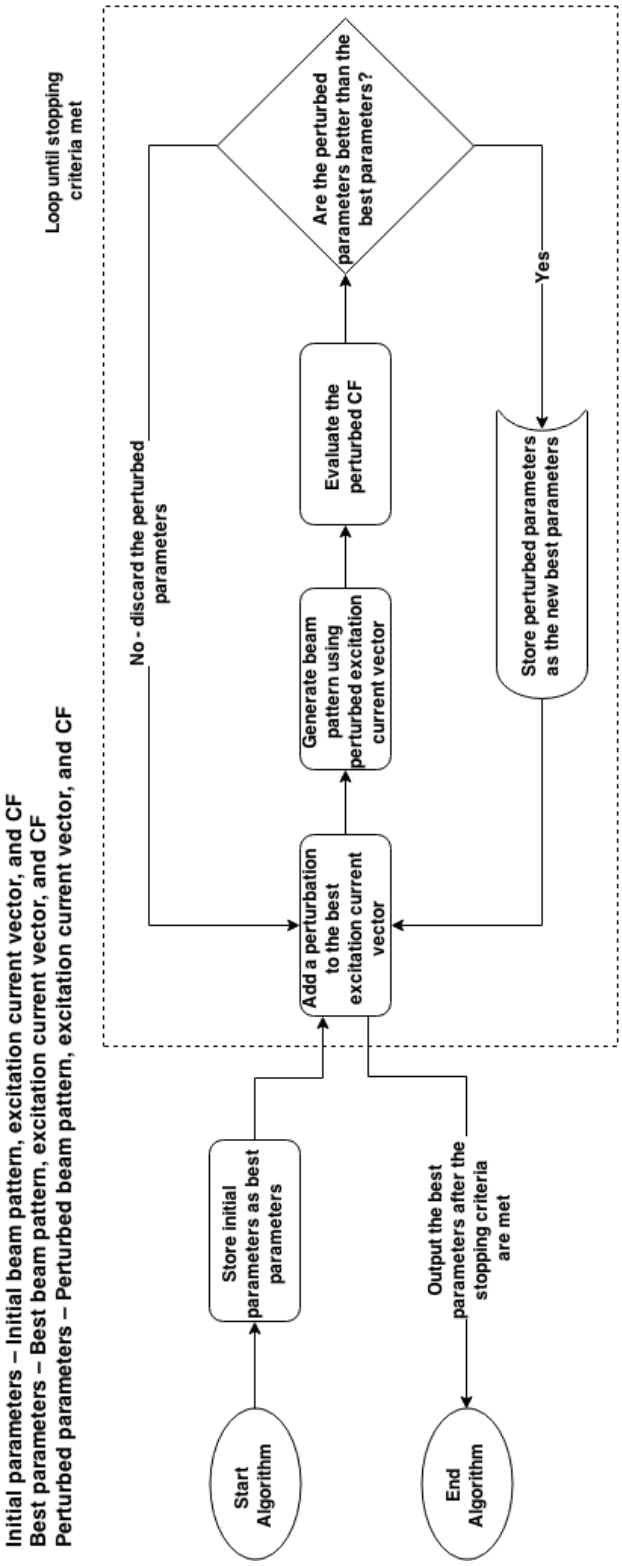

Figure 3.6.3 A flowchart representing the process undertaken by the GDA

3.7 The Metropolis Algorithm

The MA was first introduced by Metropolis, N., et al (1953) and improves on the GDA by attempting to eliminate the 'irreversible' property by which it was characterised. The MA is also a variation of the SA algorithm and operates according to a temperature profile. The MA differs primarily from the SA by the fact that it does not implement a reannealing schedule. The reannealing schedule ensures that the temperature profile of the SA is periodically reset throughout the course of the algorithm. The temperature profile allows the MA to traverse a wider search space in pursuit of an optimum excitation current vector $\vec{I}_{optimum}$ which minimises the CF. At a high temperature, the probability of the MA accepting a CF which is higher, i.e., worse than the best CF found at that point is high. The acceptance of a CF which is higher attempts to ensure that the MA does not overlook better minimum in the search space. The temperature profile decreases exponentially until it reaches a point whereby the probability of accepting a worse value is so low, that it operates similarly to the GDA outlined in Section 3.6.

The temperature profile of the MA is controlled by the variable α given by

$$\alpha = \sqrt[M]{T_{final}} \qquad \textbf{(Equation 3.7.1)}$$

where M is the maximum number of iterations set for the algorithm and T_{final} is the specified final temperature value. The temperature value at a particular iteration $m \in M$ is as follows:

$$T_m = \alpha T_{m-1} \qquad \textbf{(Equation 3.7.2)}$$

The probability of acceptance is then categorised by an exponentially decaying profile determined by α, which can be written as

$$\mathbb{P}(acceptance) = e^{\frac{-\Delta CF}{T_m \alpha}} \quad \textbf{(Equation 3.7.3)}$$

where ΔCF is the difference between the current value of the CF and the best value of the CF found at that point.

Unlike the GDA, the MA monitors three separate CFs and the corresponding excitation current vectors. The three excitation current vectors are $\vec{I}_{best}$, $\vec{I}_{current}$ and $\vec{I}_{perturbed}$ respectively. The MA stores the initial excitation current vector $\vec{I}_{initial}$ as $\vec{I}_{best}$ and $\vec{I}_{current}$. The perturbed excitation current vector is created by adding a perturbation vector $\vec{\kappa}$ to the vector $\vec{I}_{current}$ at each iteration. Similarly, as was the case in the GDA given in Section 3.6, the perturbation vector $\vec{\kappa}$ is continually scaled down in order to allow the MA to explore solutions that can only be realised by smaller excitation currents. The scaling factor should decrease according to the iteration number, and therefore it was chosen to equal the temperature value at the m^{th} iteration, T_m. The perturbed excitation current at a particular iteration m in the case of the MA is given by

$$\vec{I}_{perturbed} = T_m \vec{I}_{current} \quad \textbf{(Equation 3.7.4)}$$

The resulting beam pattern is then generated using the perturbed excitation vector $\vec{I}_{perturbed}$, and the corresponding perturbed CF is determined. The perturbed CF is then compared with the best CF in order to see if a new $\vec{I}_{best}$ has been found. If the perturbed CF is better, i.e.,

lower, than the best CF, the best parameters are overwritten with the perturbed parameters. Otherwise, a similar comparison is performed between the perturbed and current CF values.

Then, if the perturbed CF is found to be lower than the current CF, the current parameters are overwritten by the CF. However, if the perturbed CF is higher, they may be accepted and overwrite the current parameters with a probability governed by the temperature profile. Otherwise, the perturbed parameters are discarded and the algorithm reverts back to the current parameters. The steps governed by the probability of acceptance variable exemplify the explorative nature of the MA. A flowchart depicting the MA is given in Figure 3.7.2.

The exponentially decaying characteristic of the temperature profile is highly dependent on the values of M, α , $T_{initial}$ and T_{final}. The value of $T_{initial}$ sets an upper bound on the probability of acceptance and T_{final} sets a lower bound. The variable α dictates the size of the intermediate temperature values. The values used for the temperature profile for all applications of the MA are outlined in Table 3.7.1, and the corresponding temperature profile plot is given in Figure 3.7.1 for M equal to 500,000 iterations.

Table 3.7.1 Metropolis Algorithm Temperature Profile Parameters

Temperature Parameter	Value
Initial Temperature ($T_{initial}$)	0.2
Final Temperature (T_{final})	0.0001
Alpha (α)*	1

*The maximum number of iterations M for the above α value is 500,000

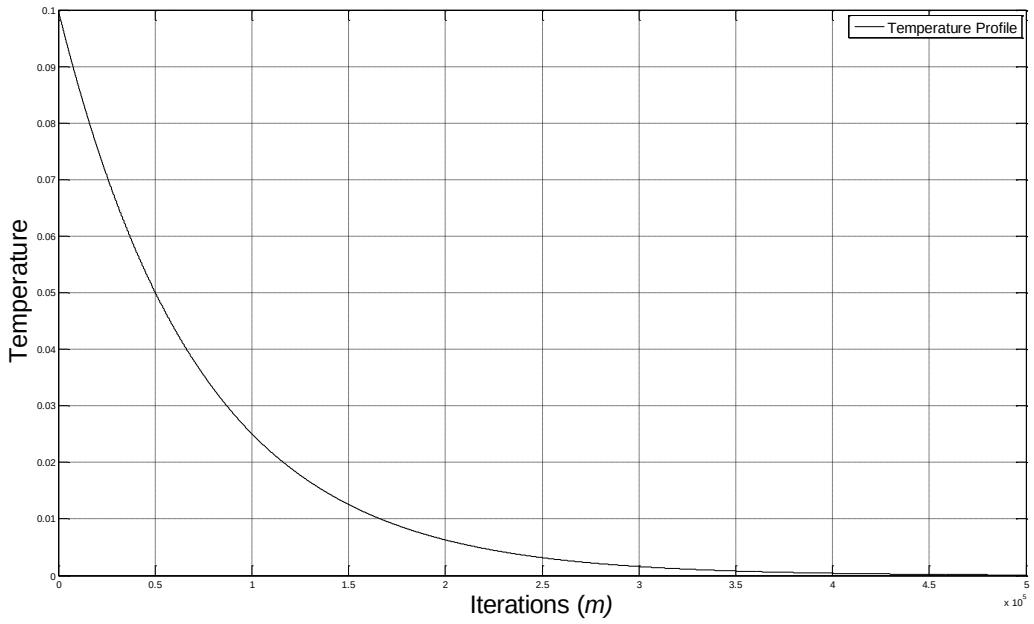

Figure 3.7.1 A plot of the temperature profile used by the MA.

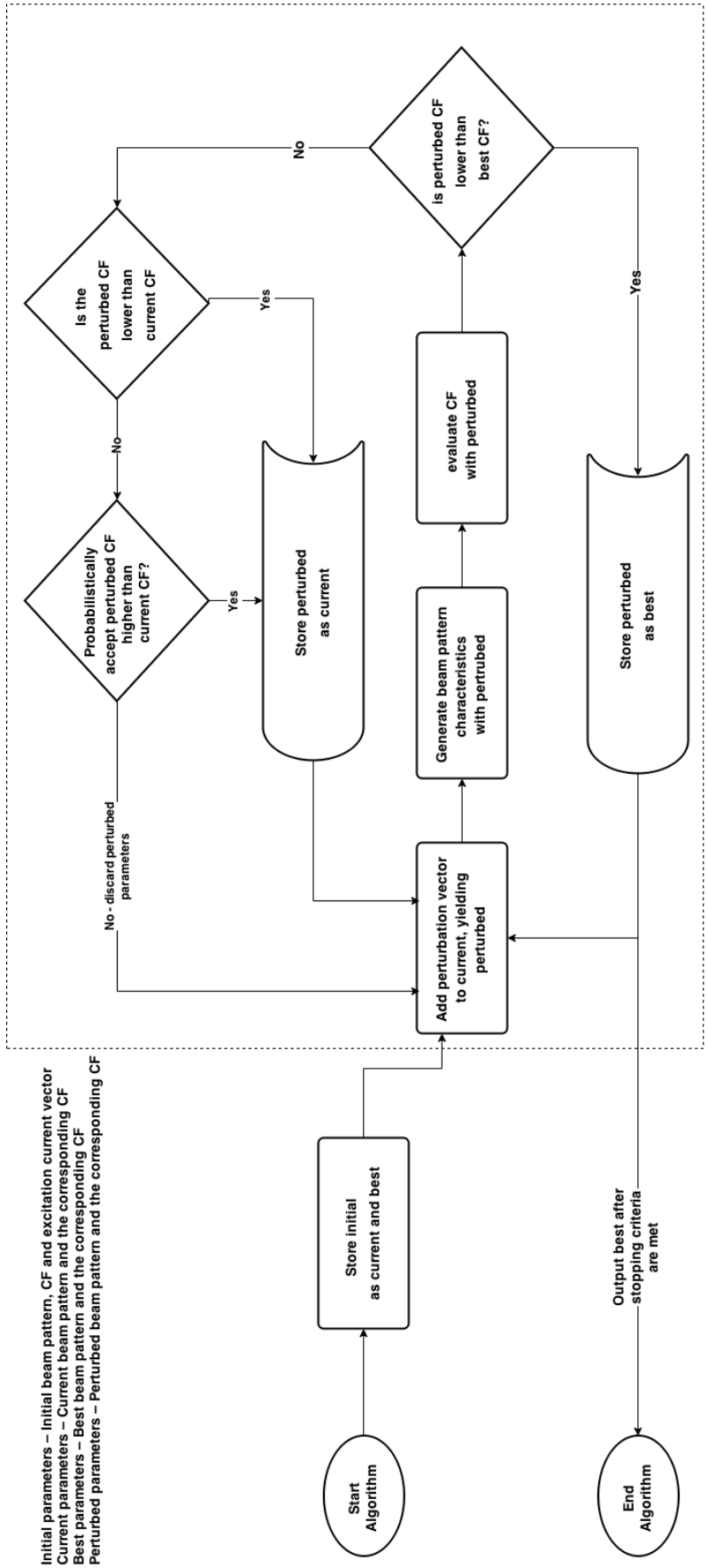

Figure 3.7.2 A flowchart outlining the process undertaken by the MA.

3.8 The Genetic Algorithm

The GA belongs to the larger set of evolutionary algorithms and is based on the process of natural selection. The GA has found applications in a number of fields, but is primarily applied to optimisation problems which have large and complex search spaces. In the GA, an initial population is continually evolved in an attempt to produce a globally optimum solution to a problem. The initial population is subjected to mutations, cross-over, and selection, as the solution progresses through generations of the algorithm in an attempt to find the globally optimum solution to the problem. The GA applied in this thesis is provided by MATLAB's Global Optimisation Toolbox (MathWorks, 2015).

The GA begins by creating a randomly generated initial population matrix of individuals, which is termed $pop_{initial}$. The random initial population ensures that each of the individuals is sufficiently different. The initial population is a $popSize \times nVar$ matrix, where $popSize$ is the number of individuals in the population and $nVar$ is the number of variables per individual. The form of the initial population is outlined in matrix form, where each row entry corresponds to an individual consisting of variables:

$$pop_{initial} = \begin{bmatrix} var_{1,1} & var_{1,2} & var_{1,3} & \dots & var_{1,nVar} \\ var_{2,1} & var_{2,2} & var_{2,3} & \dots & var_{2,nVar} \\ var_{3,1} & var_{3,2} & var_{3,3} & \dots & var_{3,nVar} \\ \vdots & \vdots & \vdots & \ddots & \vdots \\ var_{popSize,1} & var_{popSize,2} & var_{popSize,3} & \dots & var_{popSize,nVar} \end{bmatrix} \quad \textbf{(Equation 3.8.1)}$$

In the problem test cases an individual corresponds to an excitation current vector, where each row entry var represents a current feeding a sensor array element. Although not probable, it is possible that duplicate individuals exist in the initial population. The fitness of each individual is

assessed by applying the corresponding excitation current vector to the sensor array test case and calculating the corresponding CF values. These CFs are then scaled by the GA in order to converted to to a more usable range of values, known as the fitness values and given by the column vector $\vec{F}$. The scaled fitness values are stored in a $1 \times popSize$ column vector given by

$$\vec{F} = \begin{bmatrix} f_1 \\ f_2 \\ f_3 \\ \vdots \\ f_{popSize} \end{bmatrix} \quad \textbf{(Equation 3.8.2)}$$

where f corresponds to a scaled fitness value assigned to an individual of the population. The best fitness value in a population is allocated to the individual who provides the lowest CF value. In order to proceed to the next generation, the GA performs a number of computations on the current population.

The GA selects individuals, called parents, and uses these individuals to create the individuals of the subsequent population, called children. The parent selection function is stochastic and creates a line broken up into sections of varying length l, in which each parent corresponds to a section. The length of a parents section is based according to their fitness value. The parent selection function moves along the line segment in equal steps choosing the parents for the next generation. The step-size used to choose the parents is stochastically chosen by the GA. It is possible that a parent with a higher fitness value will be chosen more than once. An illustration of the selection process is detailed in Figure 3.8.1 where the length of the line segment corresponding to the highest fitness individual is denoted as l_1.

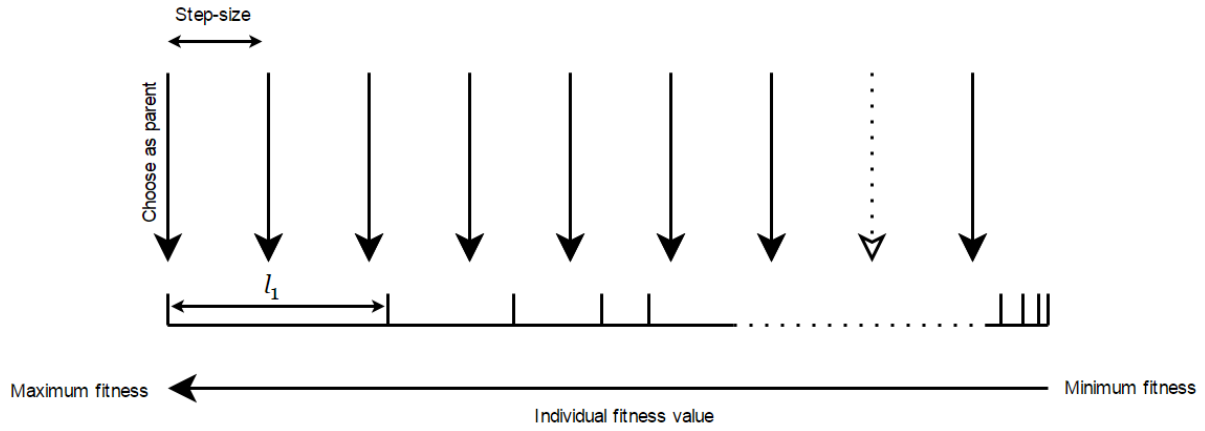

Figure 3.8.1 A diagram illustrating the stochastic parent selection procedure of the GA.

The parents chosen with the best fitness values are automatically passed to the next generation and are known as the Elite Children (EC). The number of EC is set according to the elite count variable nEC. Increasing the value of nEC can lead to the GA becoming less effective in finding an optimum solution as the fittest individuals begin to dominate the population such that the GA approximates the GDA – termed as elitism. The remaining parents undergo mutation, yielding Mutated Children (MC)–or–Crossover Children (CC).

The CC are created by combining pairs of parents in the current population, such that the resulting child is a randomly weighted average of any two randomly selected parents. The percentage of parents of a current population which pass to the next generation as CC is governed by a number between 0 and 1, called the crossover fraction. The CC is multiplied by the remaining population size having removed the EC and rounding downwards. This integer number of CC is given by

$$nCC = \lfloor (popSize - nEC)CO\% \rfloor \qquad \textbf{(Equation 3.8.3)}$$

where $CO\%$ is the crossover fraction. The remainder of the next population are made up of MC. The MC are individuals of the parents of the current population that are randomly perturbed by a random vector drawn from the Gaussian distribution. The breakdown of children that become the individuals of the next population can therefore be expressed as the sum of integer values given by

$$popSize_{next} = nEC + nCC + nMC \quad \textbf{(Equation 3.8.4)}$$

where nMC is the number of MC in the population. The GA continues the process of fitness evaluation and selection as it proceeds through the generations. The GA stops following the termination of the stopping criteria, following which the individual which resulted in the lowest CF value is returned. The returned individual is therefore also the value of the best excitation current vector $\vec{I}_{best}$. A flowchart summarising the operation of the GA is given in Figure 3.8.1.

The parameters provided to the GA in each of its applications in this thesis are outlined in Table 3.8.1. Notably, the number of EC is low relative to the number of MC and CC. This ensures that the EC do not dominate in each generation, and that the search can sufficiently traverse a greater search space as a result of it being more explorative.

Table 3.8.1 Genetic Algorithm Population and Selection Parameters

Parameter	Value
Population Size	50
Elite Count	2
Crossover Fraction	0.8
Crossover Count	38
Mutation Count	10

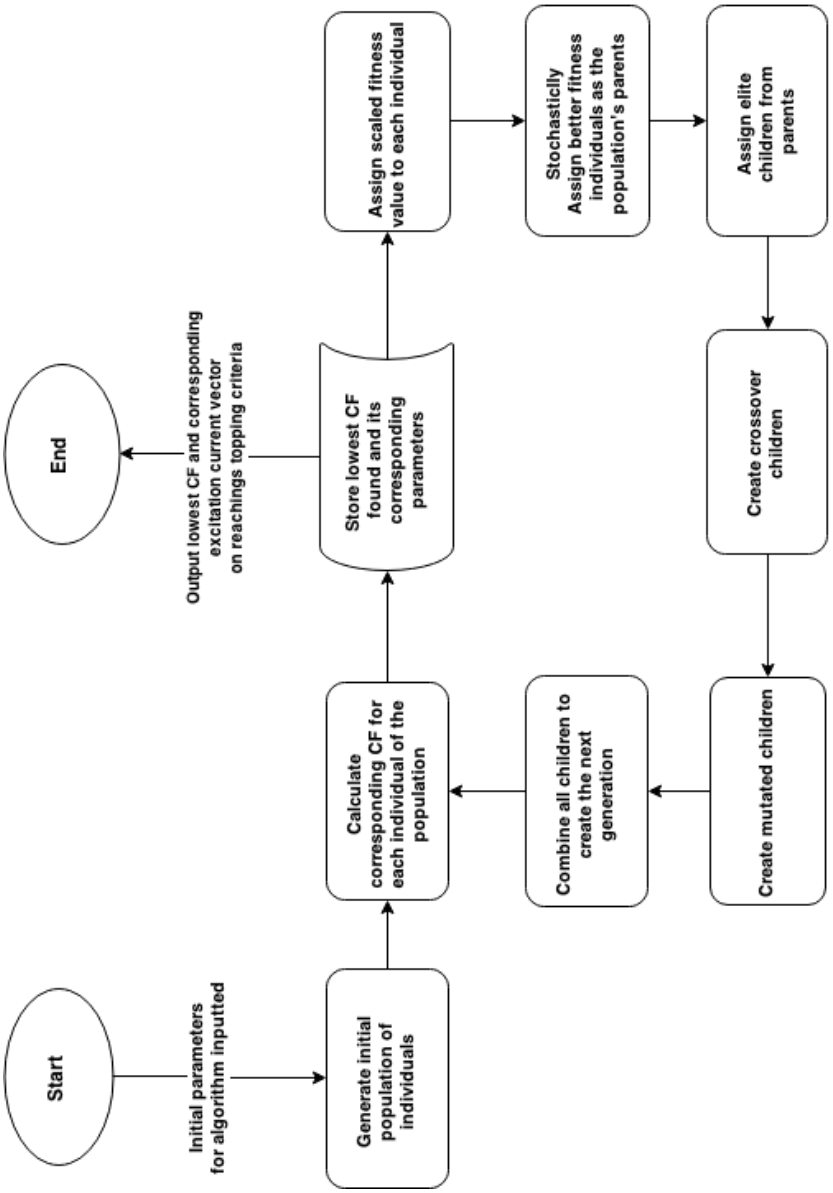

Figure 3.8.2 An outline of the process undertaken by the GA.

Chapter 4

Simulation Results

In this chapter, the results of the thesis are provided in three distinct sections and where each section corresponds to one of the three test cases examined. In each section, a short outline of all notable results is provided, which is then followed by the numerical results in tabular form. Finally, the results are provided graphically with regards to each test case. The graphical representation of the results consists of plots comparing the optimised beam patterns and the corresponding excitation current vectors for each of the experiments. The results contained in this section aim to provide an indication as to the appropriateness of the algorithms as a novel tool for beam pattern synthesis in sensor arrays.

4.1 Results of the Uniform Linear Array Test Case

In terms of complexity, the 12 element ULA was the simplest of the test cases presented. This simplicity was clearly visible by the highly symmetrical nature of the initial beam pattern which

consisted of SLs which decreased in height according to their distance from the ML (Figure 3.2.2). Thus, it can be determined that only the SLs adjacent to the ML represent a notable loss in energy. The optimisation process when applied to the ULA test case indicated that the algorithms were capable of a high degree of optimisation. The results also suggested that the optimised beam patterns were approaching an optimal pattern. This is due to the resultant beam patterns resembling the pattern produced by the D-C method in which all of the SLs are at an equal level (Figure 2.2.1). However, the optimality of the solution is unable to be confirmed due to the vastness of the search space, and in which no known optimum solution exists. The numerical results obtained for the ULA test case are detailed in Table 4.1.1.

Initially, the timed experiments which were completed using both bounded and unbounded current excitations indicated that a decrease in the max SL of 10 dB to -23 dB from an initial maximum SL of -13.06 dB was realisable in the given time limit of 1500 seconds. The lowest SL height encountered was -23.70 dB down from the ML and was found using the GDA with bounded currents. The MA was found to perform similarly in the same experiment with a beam pattern in which the maximum SL was -23.68 dB. The GA provided the lowest CF value in the 1500 seconds which resulted in a maximum SL of -23.06 dB down from the ML. A similar trend was apparent in the timed experiments using unbounded currents. The GDA was again shown to outperform the MA and GA, producing a beam pattern with a maximum SL of -23.69 dB. The corresponding MA and GA solutions produced maximum SLs of -23.58 dB and -22.58 dB respectively. A plot illustrating the beam patterns of the timed experiments with bounded and unbounded currents is given in Figures 4.1.1 and 4.1.3.

The excitation current vectors for the timed-unbounded current experiments were also analysed in order to distinguish if the resulting values were applicable in practice. Generally, the unbounded current norms were normal relative to the initial current norm. However, this was not the case in regards to the MA in the timed-unbounded current experiment which produced a current norm of 84.3304. This current norm value is over 20 times larger than the initial current excitation vector norm. The current norms in the bounded-current case were found to be reasonable due to the applied current constraints. Scatter plots illustrating the final excitation current vectors are provided in Figures 4.1.2 and 4.1.4.

The performance based experiments were also indicative that the algorithms were capable of reaching a target CF of 0.075 in the ULA test case. However, the times taken to achieve this target CF were found to vary between the algorithms. The initial ULA beam pattern produced an initial CF value of 0.2222 such that a reduction of 0.1472 was required. In terms of optimisation time, the GDA was found to be the quickest in both the bounded and unbounded test cases with 2.0271 seconds and 2.1609 seconds. The optimisation using the MA was slightly slower with 4.3253 seconds and 4.9495 seconds. However, the GA was the least effective in terms of time with 5.8901 seconds and 254.237 seconds respectively. Comparison plots of the algorithms in the performance based tests are given in Figures 4.1.5 and 4.1.7.

Again, and as was the case with the unbounded-timed experiments, the MA produced a very large current norm. The current norm produced by the MA increased to 36.2089 in 4.9495 seconds. It is evident that the MA naturally increases the values of the excitation currents to possibly unrealistic values in the unbounded experiments. All other current norms produced

were at adequate levels for the simulations. Plots illustrating the excitation current level can be given in Figures 4.1.6 and 4.1.8.

Table 4.1.1 Results of ULA Test Case

a. Unbounded Currents – Time Limit

	Max SL (dB)	Max SL	ML	CF	Iterations/Generations	Time (seconds)	Current Norm
Initial	-13.06	2.6668	12.0000	0.2222	-	-	3.4641
GDA	-23.69	3.6969	56.5452	0.0654	540270	1500	16.9715
MA	-23.58	18.5931	280.639	0.0663	655897	1500	84.3304
GA	-22.58	0.8171	10.9910	0.0743	490182	1500	3.3285

b. Unbounded Currents – Minimum CF Target

	Max SL (dB)	Max SL	ML	CF	Iterations/Generations	Time (seconds)	Current Norm
Initial	-13.06	2.6668	12.0000	0.2222	-	-	3.4641
GDA	-22.58	2.3381	31.2282	0.0750	17746	2.1609	9.4416
MA	-22.51	8.9759	119.7020	0.0750	46123	4.9495	36.2089
GA	-22.57	4.4881	60.2725	0.0750	66458	254.2327	18.1695

c. Bounded Currents – Time Limit

	Max SL (dB)	Max SL	ML	CF	Iterations/Generations	Time (seconds)	Current Norm
Initial	-13.06	2.6668	12.0000	0.2222	-	-	3.4641
GDA	-23.70	3.1014	47.4894	0.0653	561813	1500	14.2492
MA	-23.68	3.2697	49.9572	0.0655	585068	1500	14.9936
GA	-23.06	2.8167	40.0839	0.0703	489567	1500	12.0797

d. Bounded Currents – Minimum CF Target

	Max SL (dB)	Max SL	ML	CF	Iterations/Generations	Time (seconds)	Current Norm
Initial	-13.06	2.6668	12.0000	0.2222	-	-	3.4641
GDA	-22.56	4.0921	54.9629	0.0750	18095	2.0271	16.5789
MA	-22.53	4.1900	56.0446	0.0750	37880	4.3253	16.9274
GA	-22.50	2.2084	29.4532	0.0750	934	5.8901	8.9119

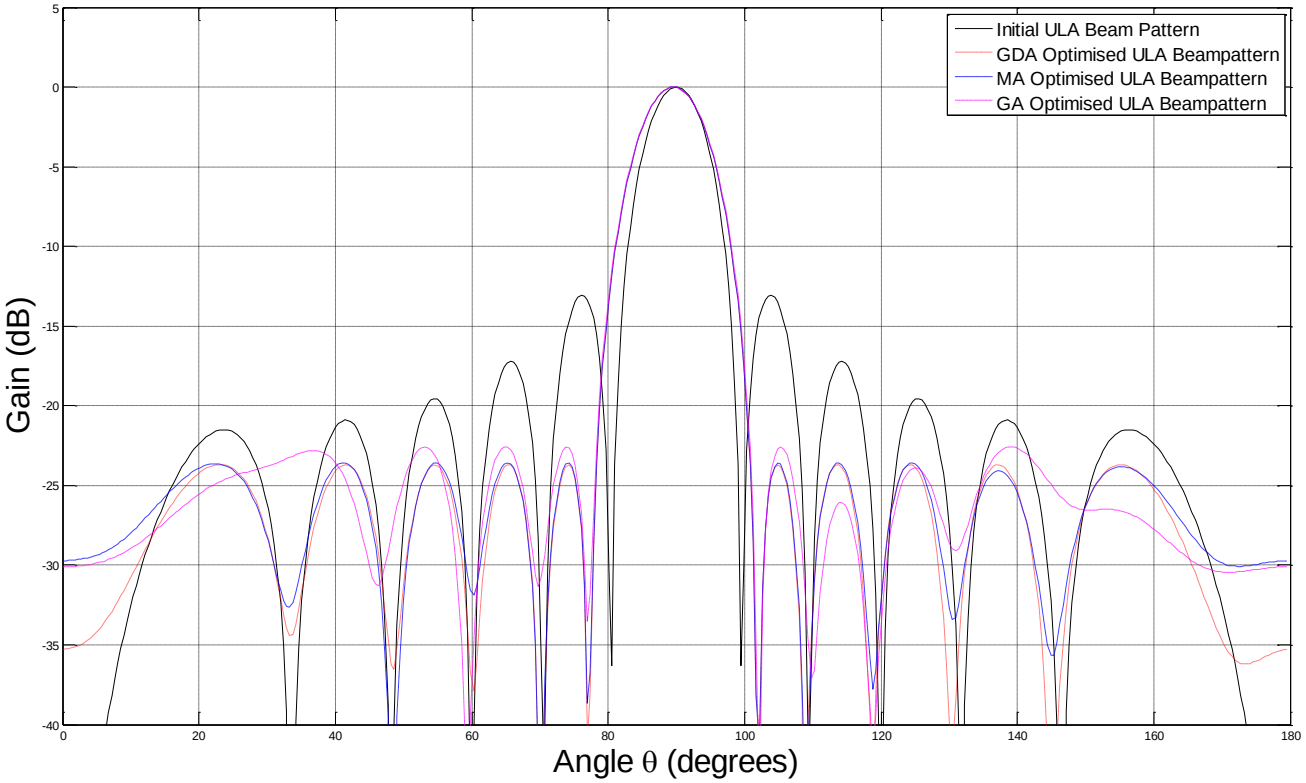

Figure 4.1.1 A plot comparing the initial and optimised beam patterns for the ULA in the timed-unbounded experiment.

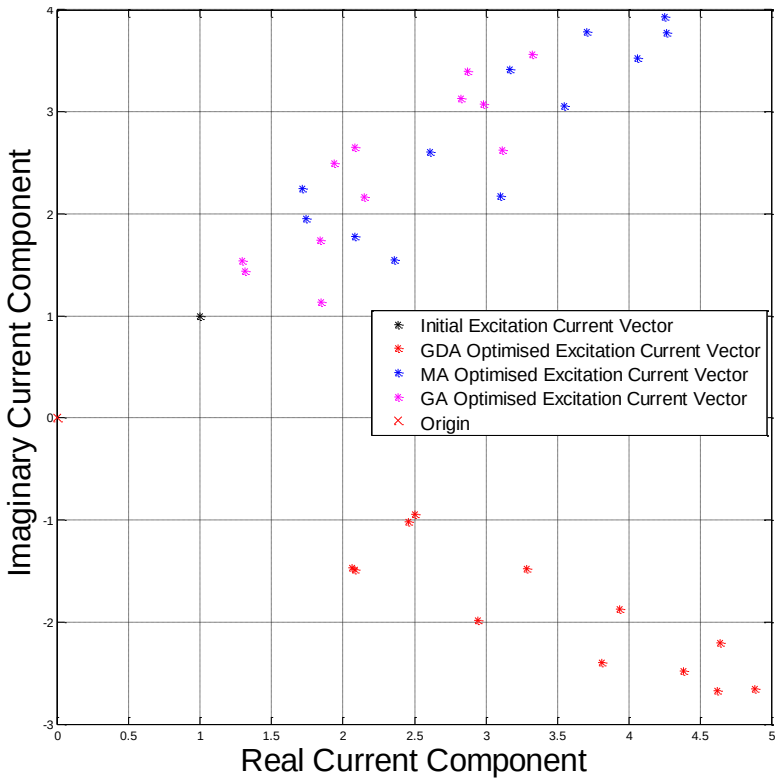

Figure 4.1.2 A scatter plot comparing the initial and optimised excitation current vectors for the ULA in the timed-unbounded experiment.

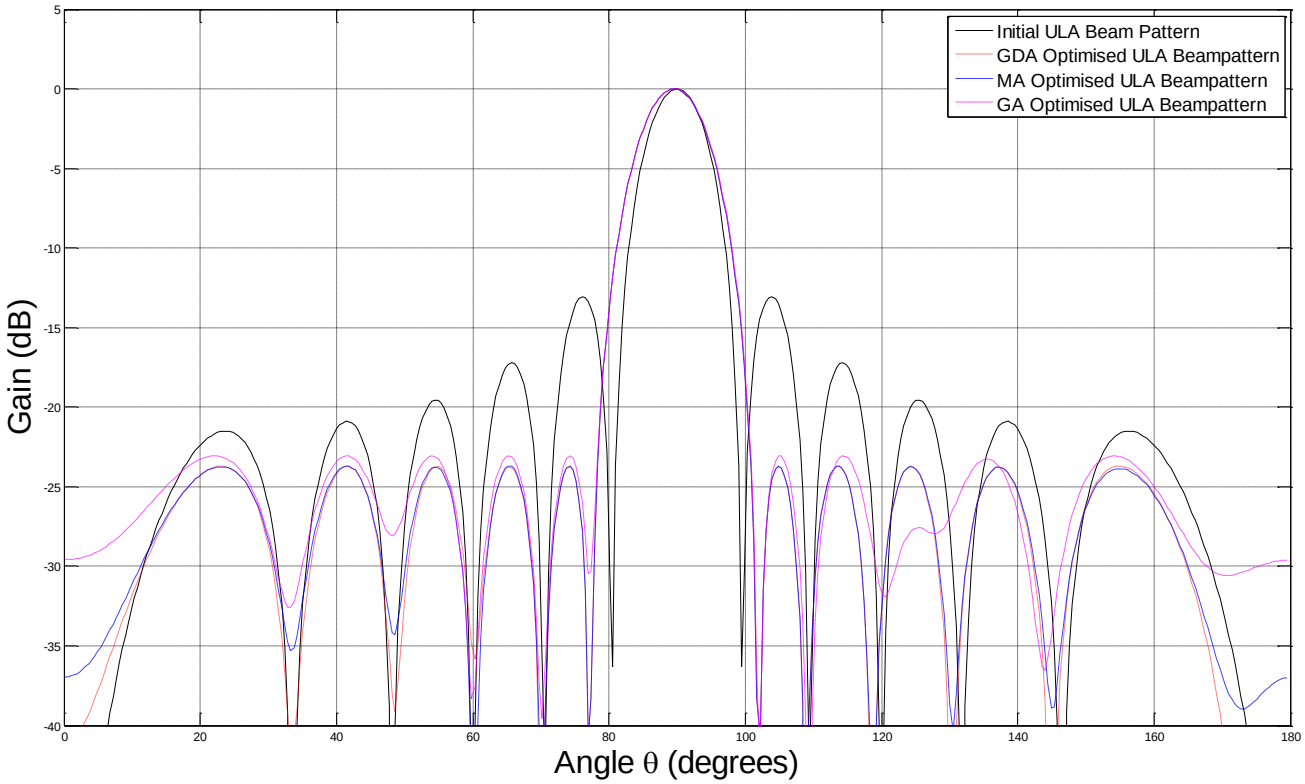

Figure 4.1.3 A plot comparing the initial and optimised beam patterns for the ULA in the timed-bounded experiment.

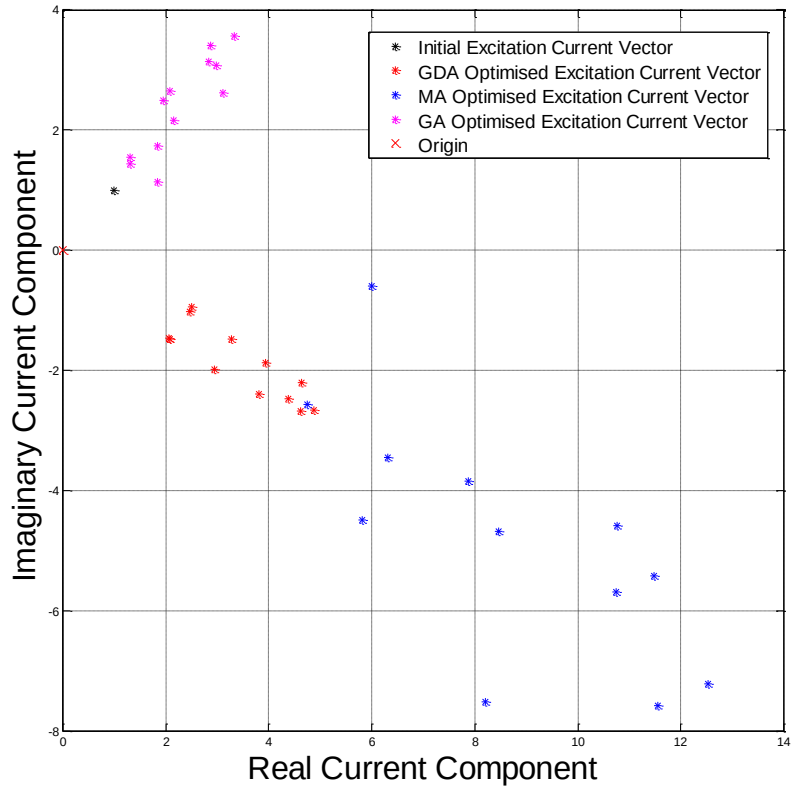

Figure 4.1.4 A scatter plot comparing the initial and optimised excitation current vectors for the ULA in the timed-bounded experiment.

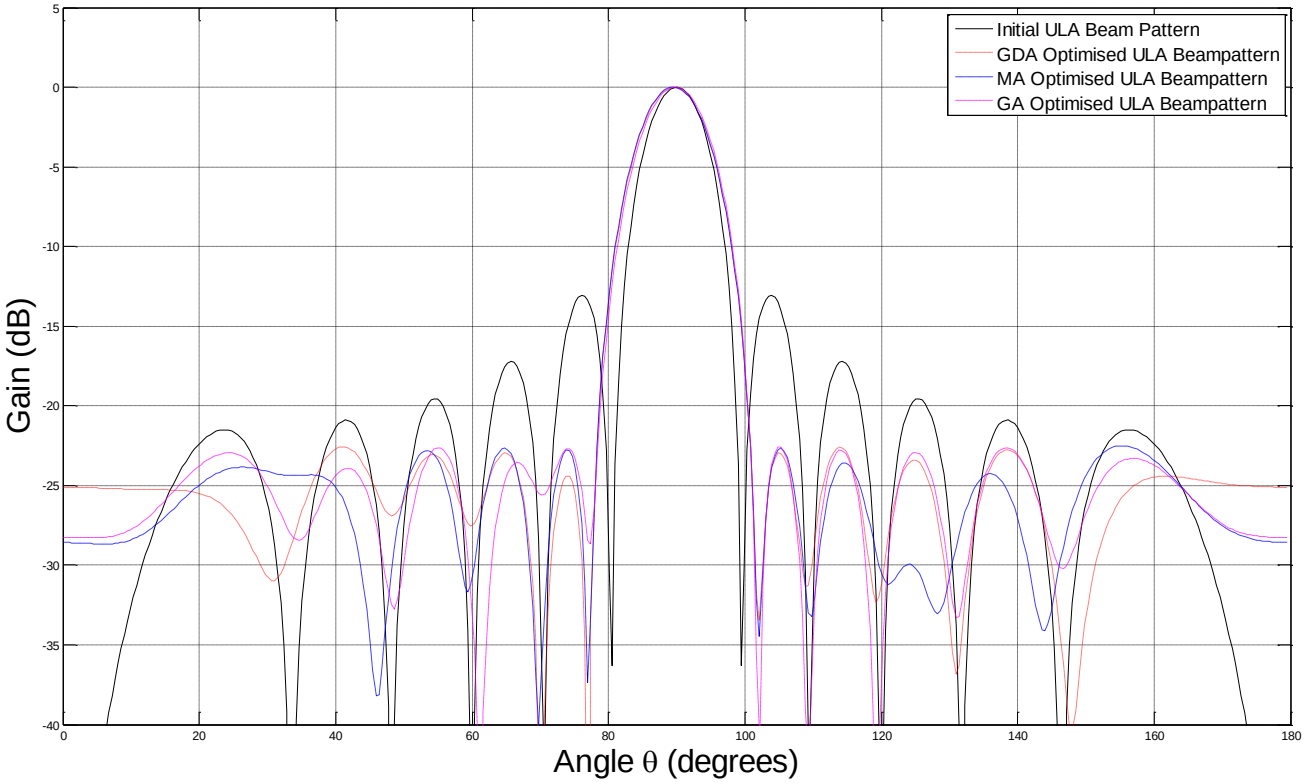

Figure 4.1.5 A plot comparing the initial and optimised beam patterns for the ULA in the minimum target CF-unbounded experiment.

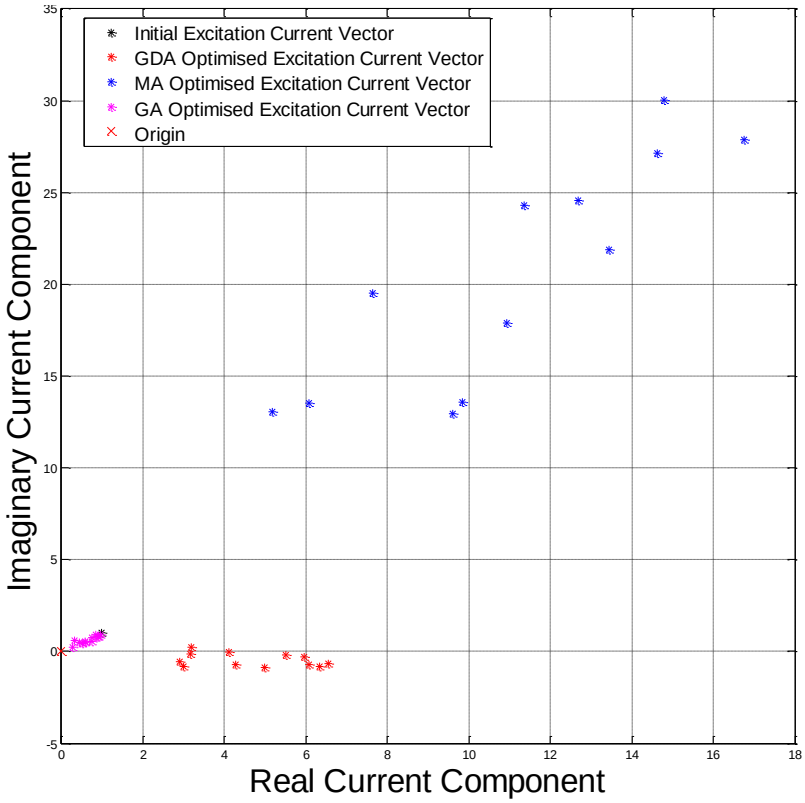

Figure 4.1.6 A scatter plot comparing the initial and optimised excitation current vectors for the ULA in the minimum target CF-unbounded experiment.

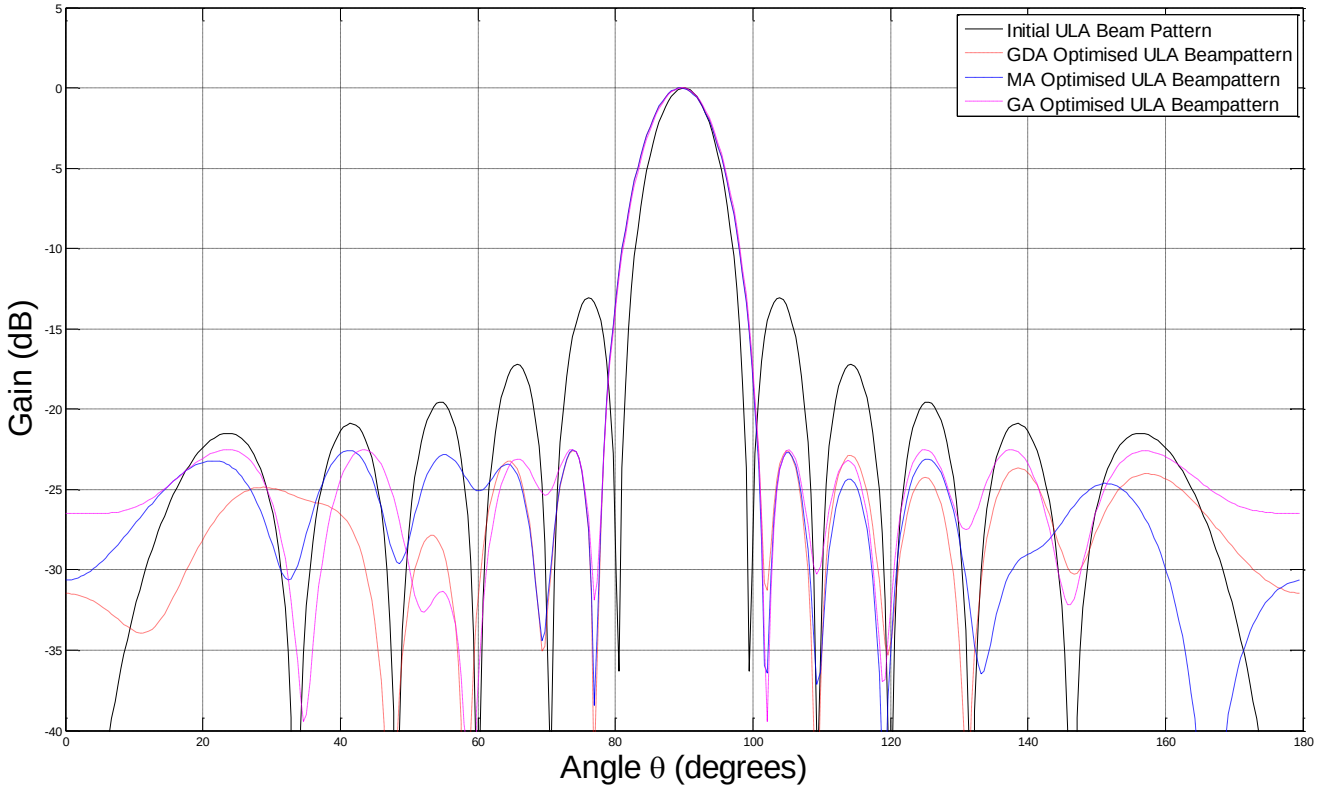

Figure 4.1.7 A plot comparing the initial and optimised beam patterns for the ULA in the minimum target CF-bounded experiment.

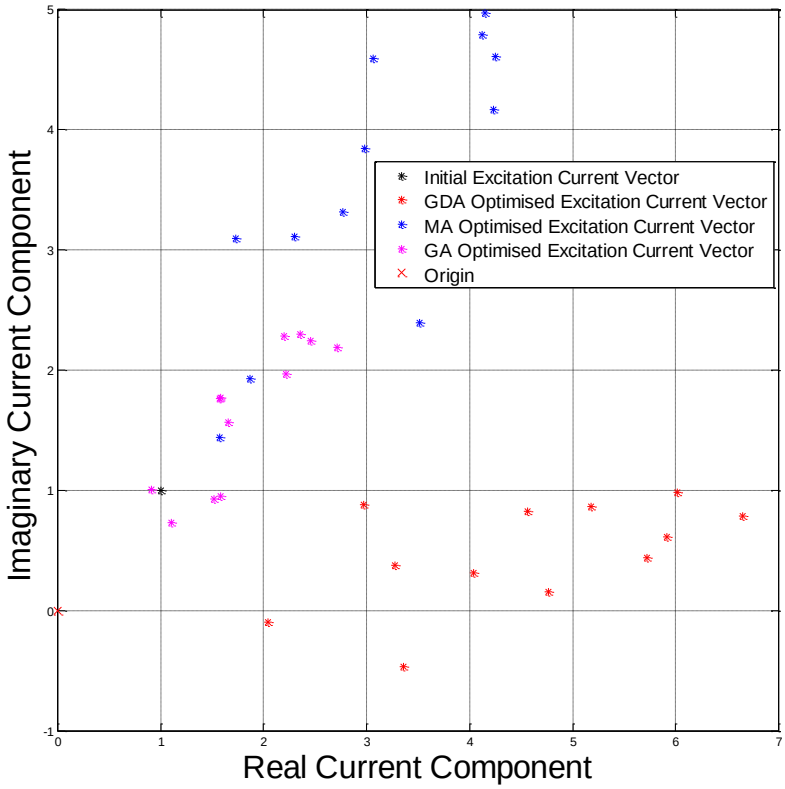

Figure 4.1.8 A scatter plot comparing the initial and optimised excitation current vectors for the ULA in the minimum target CF-bounded experiment.

4.2 Results of the Uniform Linear Array with an Inactive Element Test Case

The ULA with an inactive element aimed to introduce an increased degree of complexity to the optimisation process. The loss of an element had an adverse effect on the resulting beam pattern such that the SLL decreased significantly (Figure 3.3.1). This decrease in SLL corresponds to a high CF value and is indicative that an increased amount of radiation is being transmitted in unwanted directions. A table of numerical results is provided in Table 4.2 and details the effectiveness of the applied algorithms in each of the experiments. The experiments showed that the GDA, MA, and GA were capable of providing optimisation to the beam pattern of a sensor array following the loss of an element.

The applied algorithms provided a similar degree of optimisation in each the timed experiments with a reduction in the max SL of approximately -5.5 dB being shown as reasonable. However, the timed results indicated that the MA and GDA are capable of providing a much greater level of optimisation, when compared with the GA. The unbounded experiment saw the MA and GDA produce CF solutions which corresponded to a maximum SL height of -15.44 dB and -15.56 dB. This is in contrast to the GA which produced a CF which only resulted in a maximum SL of -15.14 dB. Similarly in the bounded case, the GA again performed the poorest of the three algorithms in the given time limit with a maximum SL of -15.31 dB. The optimised maximum SL of the GDA and MA may not appear entirely different to the value of the GA's maximum SL of -15.54 dB and -15.56 dB, but it is significant in relative terms in indicating that the GA may not be suitable for the beam pattern synthesis problems provided. A number of plots comparing the optimised beam patterns are given in Figures 4.2.1 and 4.2.3.

The excitation current vector plots showed a similar trend to the results of the ULA test case given in Section 4.1. As expected, the current excitation vector in the bounded experiments was sufficiently constrained such that the values remained more realistic (Figure 4.2.4). This was also found to occur in the beam patterns optimised by the GDA and GA in the unbounded current cases. It is noted that the MA again produces large excitation current values. This is highlighted by the results of the unbounded test case where the current norm is high at 147.3132. This is considerably large when compared with the current norms of the GDA and GA which are 16.2140 and 3.9283 respectively. These differences are particularly visible in Figure 4.2.2 where the excitation currents provided by the MA are located a significant distance from the initial current excitation vector norm.

The minimum target CF performance based experiments indicated short optimisation times were possible with the GDA and MA. The minimum CF value of 0.1800 required a reduction of 0.1486 from the initial CF of 0.3286. It was found that the time required to reduce the CF to the target value varied according to the algorithm. The GDA proved to be the quickest in both the unbounded and bounded current experiments, reaching the target CF in a time of 1.6608 seconds and 2.0015 seconds. The MA optimisation process was slower with 20.0258 and 2.1899 seconds for the same experiments. However, the GA reached the specified CF target in the slowest time of 47.0169 seconds and 31.6699 seconds. The current norms were acceptable in the case of the bounded experiments, and also the unbounded experiments when the GDA or GA was used. The MA produced a large current norm of 72.360 which may offer an explanation for the optimisation time of 20.0258 seconds. The growth in the size of the excitation current vector may adversely affect the ability of the MA in quickly minimising the CF. The resulting

beam patterns are compared in Figures 4.2.5 and 4.2.7, whereas the corresponding current values are outlined in Figures 4.2.6 and 4.2.8.

Table 4.2.1 Results of ULA with an Inactive Element Test Case

a. Unbounded Currents – Time Limit

	Max SL (dB)	Max SL	ML	CF	Iterations/Generations	Time (seconds)	Current Norm
Initial	-9.67	3.6149	11.0000	0.3286	-	-	3.3166
GDA	-15.56	8.1380	48.7986	0.1668	561374	1500	16.2140
MA	-15.44	76.3176	451.3878	0.1691	584132	1500	147.3132
GA	-15.14	2.0991	12.0005	0.1749	440148	1500	3.9283

b. Unbounded Currents – Minimum CF Target

	Max SL (dB)	Max SL	ML	CF	Iterations/Generations	Time (seconds)	Current Norm
Initial	-9.67	3.6149	11.0000	0.3286	-	-	3.3166
GDA	-14.94	5.5027	30.7349	0.1800	12813	1.6608	10.0862
MA	-14.89	40.3443	224.1454	0.1800	80334	20.0258	72.360
GA	-14.89	1.7177	9.5455	0.1800	8424	47.0169	3.0664

c. Bounded Currents – Time Limit

	Max SL (dB)	Max SL	ML	CF	Iterations/Generations	Time (seconds)	Current Norm
Initial	-9.67	3.6149	11.0000	0.3286	-	-	3.3166
GDA	-15.54	4.8106	28.8010	0.1670	543654	1500	9.4732
MA	-15.56	6.8512	41.005	0.1667	524841	1500	13.4615
GA	-15.31	1.6518	9.6279	0.1716	452793	1500	3.1104

d. Bounded Currents – Minimum CF Target

	Max SL (dB)	Max SL	ML	CF	Iterations/Generations	Time (seconds)	Current Norm
Initial	-9.67	3.6149	11.0000	0.3286	-	-	3.3166
GDA	-14.97	6.2087	34.7926	0.1800	13801	2.0015	11.1678
MA	-14.91	6.4589	35.9291	0.1800	20922	2.1899	11.6031
GA	-14.90	1.7177	9.5455	0.1800	6427	31.6699	3.0664

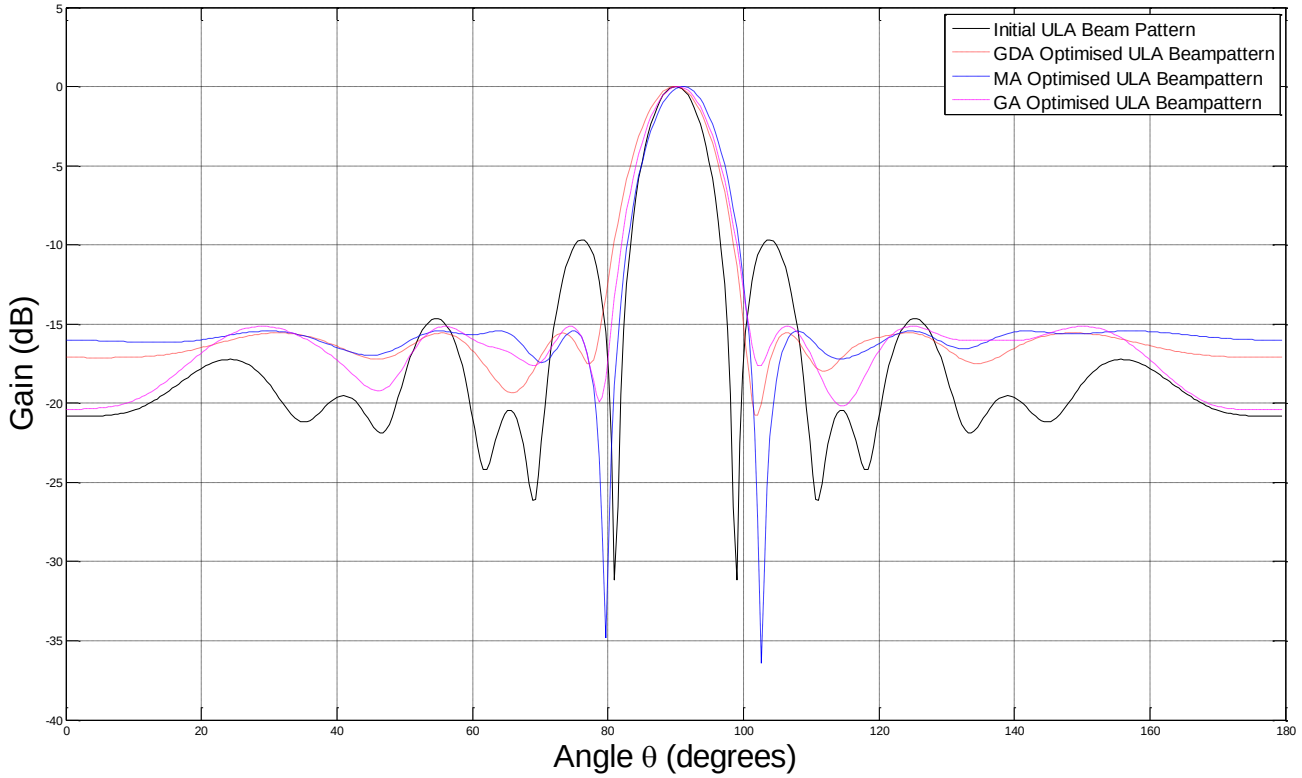

Figure 4.2.1 A plot comparing the initial and optimised beam patterns for the ULA with an inactive element in the timed-unbounded experiments.

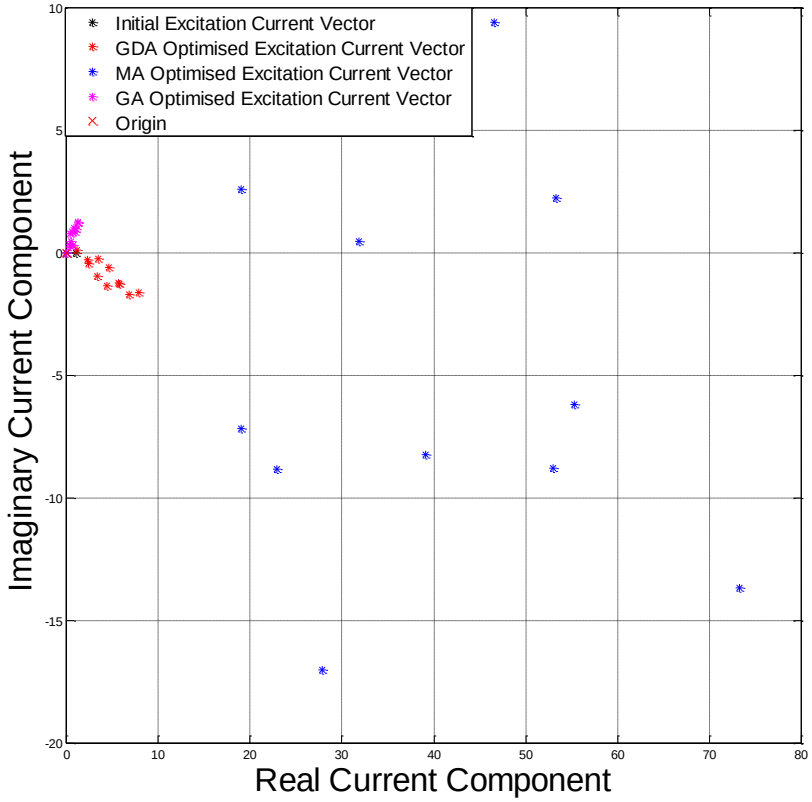

Figure 4.2.2 A scatter plot comparing the initial and optimised excitation current vectors for the ULA with an inactive element in the timed-unbounded experiments.

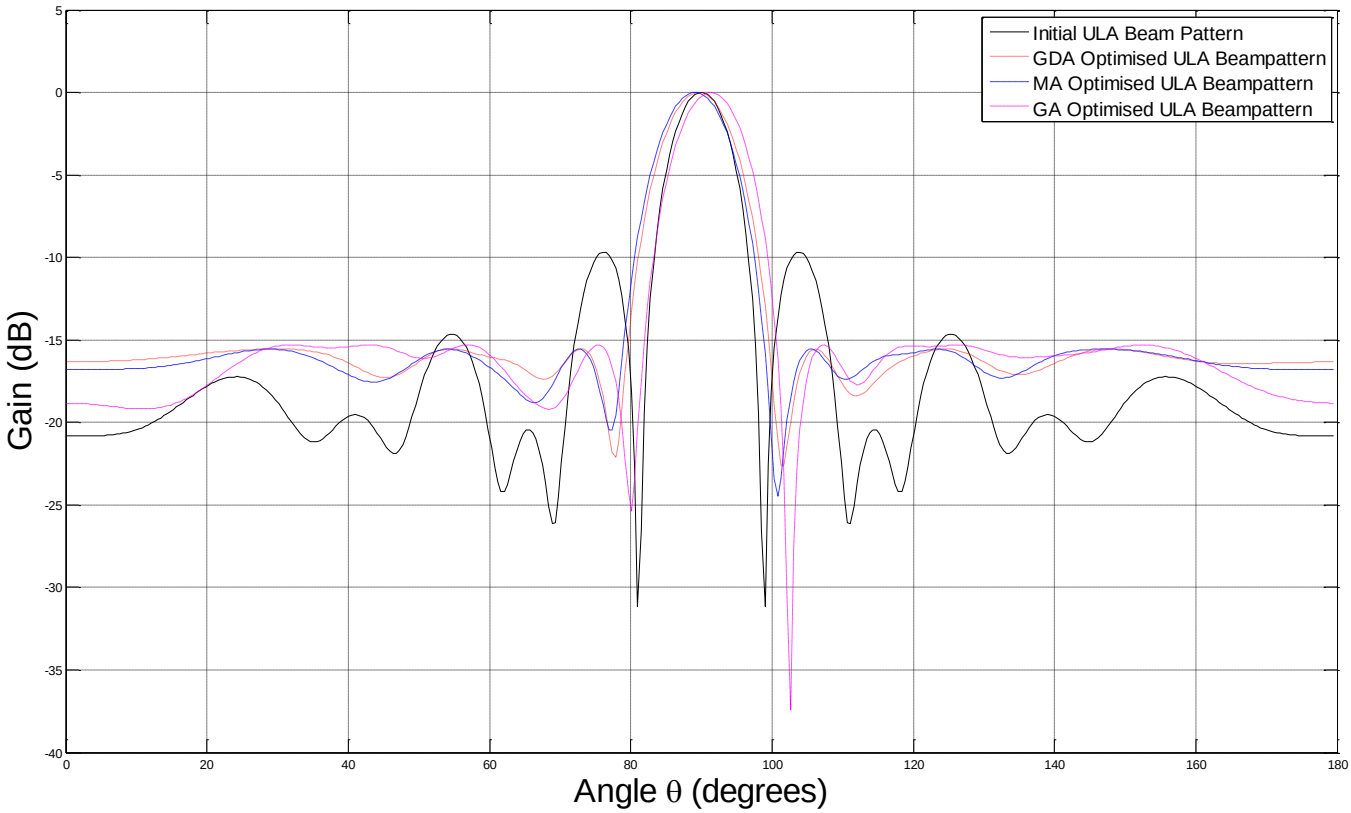

Figure 4.2.3 A plot comparing the initial and optimised beam patterns for the ULA with an inactive element in the time-bounded experiments.

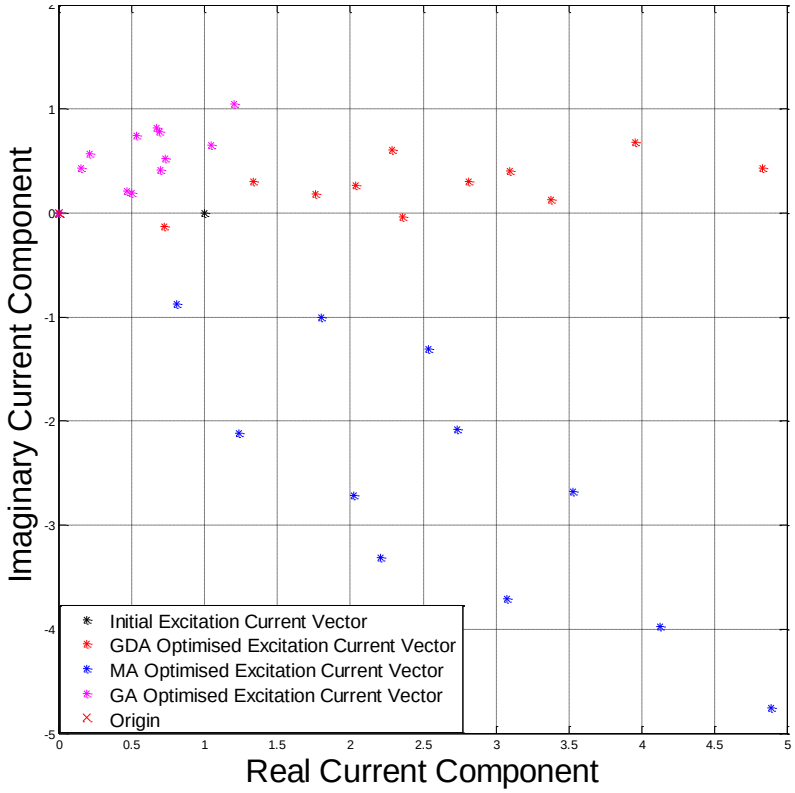

Figure 4.2.4 A scatter plot comparing the initial and optimised excitation current vectors for the ULA with an inactive element in the timed-bounded experiments.

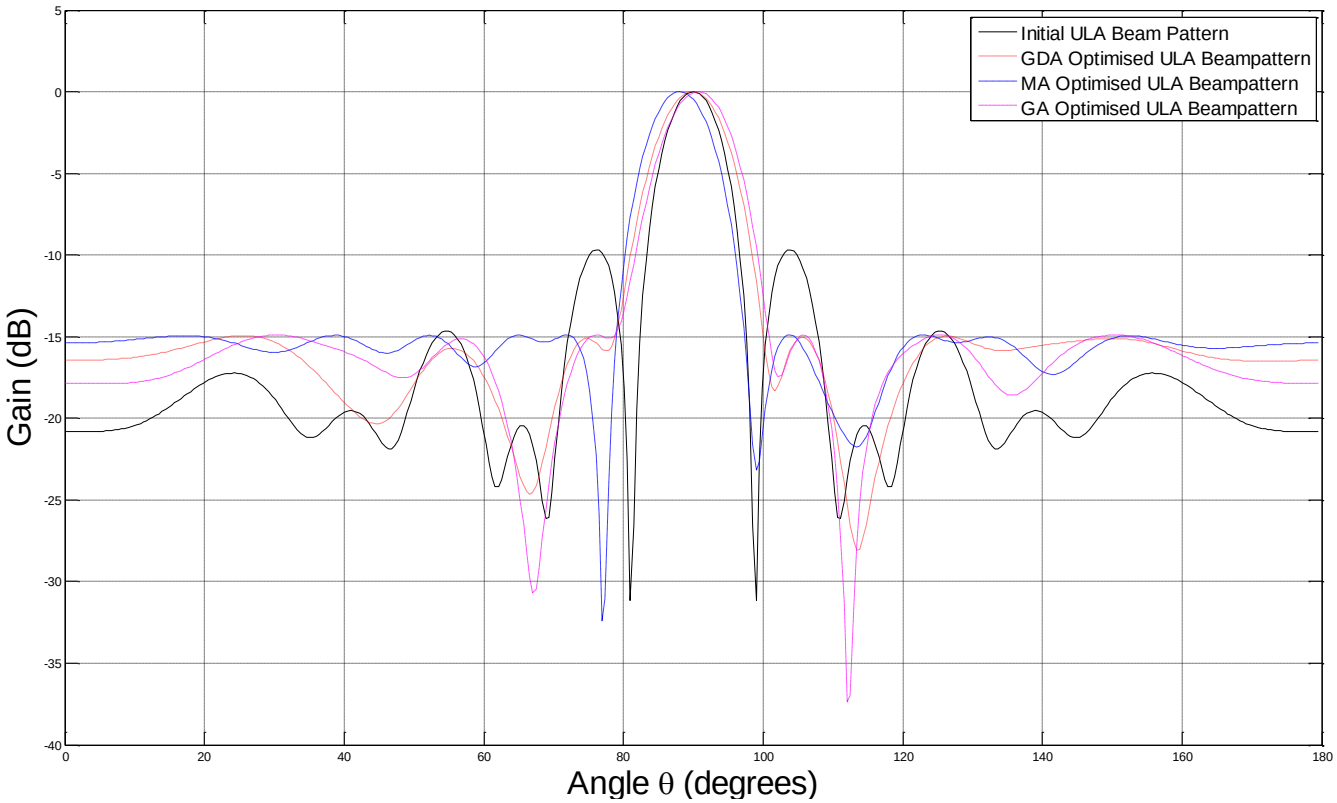

Figure 4.2.5 A plot comparing the initial and optimised beam patterns for the ULA with an inactive element in the minimum target CF-unbounded experiments.

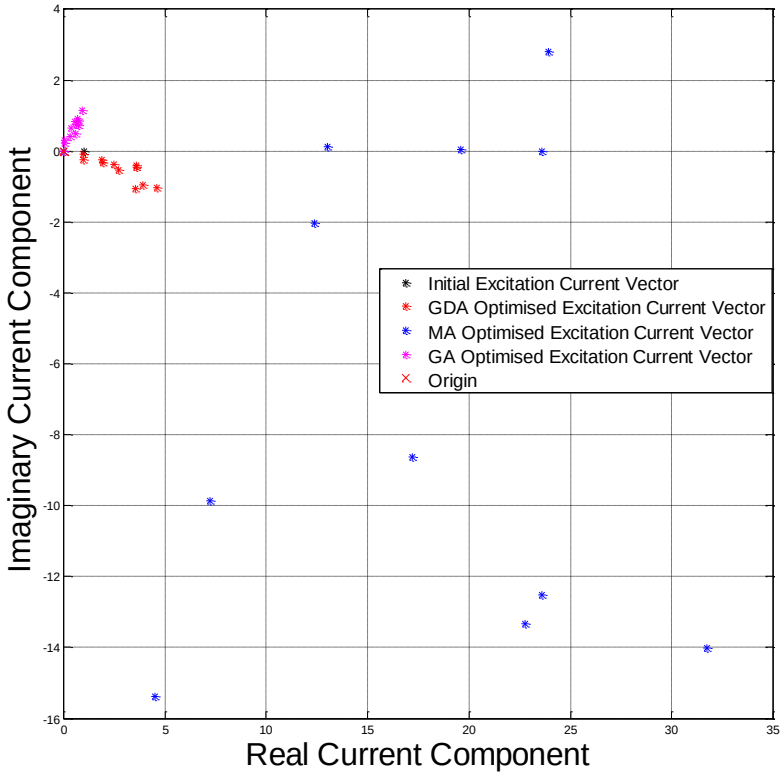

Figure 4.2.6 A scatter plot comparing the initial and optimised excitation current vectors for the ULA with an inactive element in the minimum target CF-unbounded experiments.

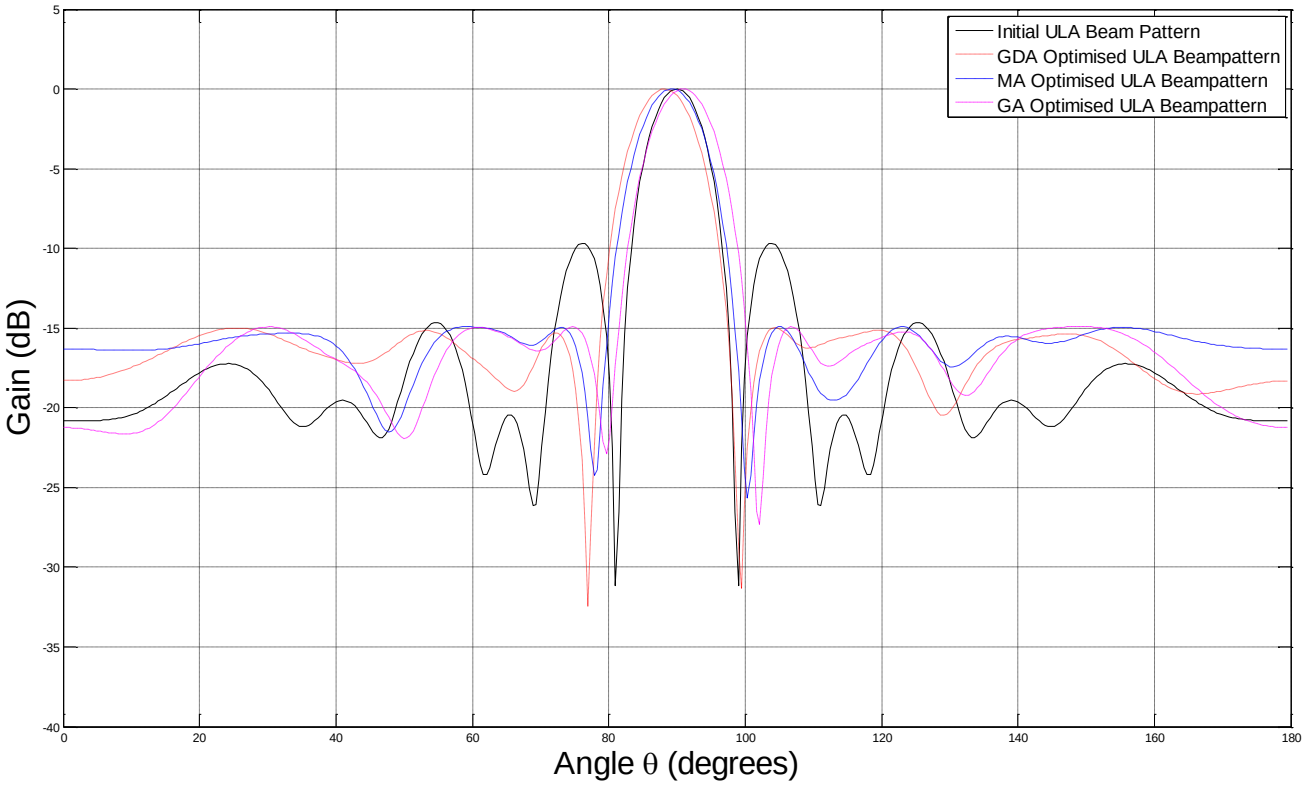

Figure 4.2.7 A plot comparing the initial and optimised beam patterns for the ULA with an inactive element in the minimum target CF-bounded experiments.

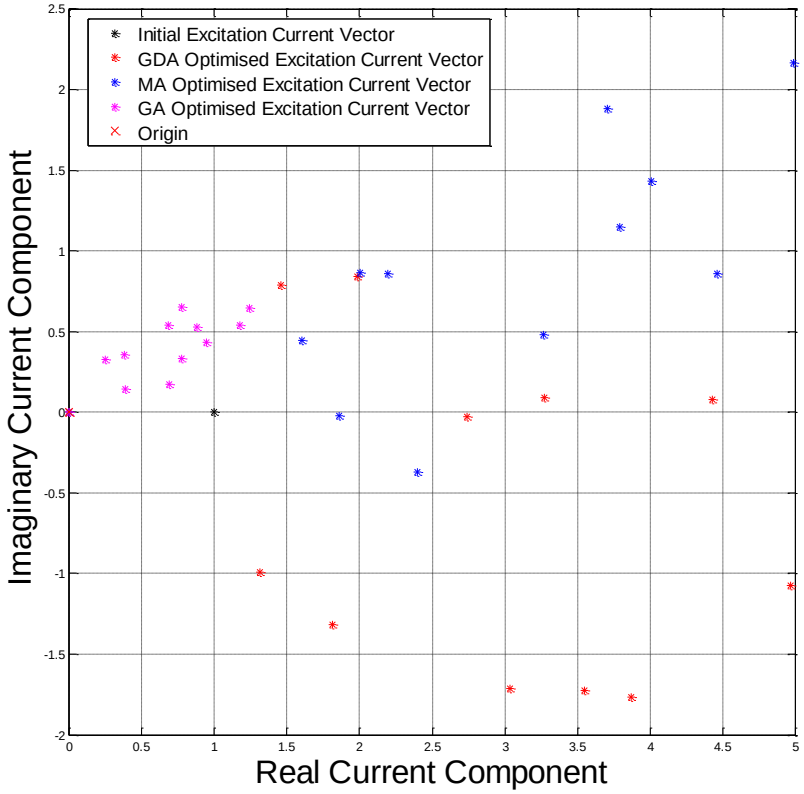

Figure 4.2.8 A scatter plot comparing the initial and optimised excitation current vectors for the ULA with an inactive element in the minimum target CF-bounded experiments.

4.3 Results of the Wireless Sensor Network Array Test Case

The randomly generated WSN array of 32 elements provided the most complex beam pattern of the three test cases. The initial beam pattern, which remained constant throughout each of the experiments, is highly asymmetrical in nature. Moreover, a number of distinct SLs are also visible, which required suppression in order to reduce energy loss. The successful suppression of the SLs of the WSN array's beam pattern would showcase the flexibility of the algorithms that have been outlined.

The timed experiments, which allowed each of the algorithms to run for 1500 seconds with both bounded and unbounded currents, provided CF solutions of varying quality. The lowest CF solution in the unbounded current experiment was found by the GDA, which resulted in a beam pattern with a maximum SL of -26.09 dB. This maximum SL figure is significantly lower than those of the MA and GA at -17.66 dB and-14.59 dB. In the bounded current test, the MA was capable of outperforming both the GDA and the GA with a maximum SL of -23.80 dB. The GDA provided a similar level of SL reduction with a maximum SL of-22.55 dB. Lastly, the GA provided an excitation current vector which resulted in a maximum SL of -9.381 dB and in this case, a value which indicates that the GA is the least capable of the three algorithms in providing an optimised pattern. A comparison of the beam patterns for the case of the WSN array is provided in Figures 4.3.1 and 4.3.3.

The excitation current vectors were analysed and were found to be abnormal in the unbounded MA case with a current norm of 160.574. The remaining experiments, including the MA with bounded currents, provided excitation current vectors which would be considered realistic. The

excitation current vectors are outlined in Figures 4.3.2 and 4.3.4, where the initial excitation current vector is represented by a circular excitation pattern encircling the origin, which indicates that the beam array is steered at 180°.

The importance of the performance based experiments in regards to the WSN array stems from the fact that, in theory, dynamical sensor elements could collaborate in order to form a distributed array. Thus, it would be expected that any applied beam pattern synthesis procedure is efficient in terms of providing quick and efficient SL reduction according to changes in the sensor array. The bounded and unbounded experiments were, in general, positive in indicating that the algorithms are sufficiently flexible in achieving this.

The positive results are primarily apparent when the GDA and MA were analysed. The GDA and MA provide a solution equal to the target CF in the bounded experiment of 0.2 in 2.7931 seconds and 1.4964 seconds respectively. The GDA provided a similar result in the unbounded case where a solution equalling the target CF was found in 0.2323 seconds; however, this target CF proved an issue for the MA which was unable to produce an adequate solution until 212.159 seconds. Moreover, this resulted in a large current norm of 462.584. The GA was capable of producing a solution in 18.9389 seconds in the unbounded case, however the GA was found to be unable to reach the target CF in the bounded current case. The GA was allowed to run for 3600 seconds (60 minutes) in an attempt to reach the target CF, but it was only capable of reducing the CF value to 0.2953. The comparison plots of the optimised beam patterns for the target CF experiment in the case of the WSN array are given in Figures 4.3.5 and 4.3.7. The corresponding excitation current plots are also provided in Figures 4.3.6 and 4.3.8.

Table 4.2.1 Results of the WSN Array Test Case

a. Unbounded Currents – Time Limit

	Max SL (dB)	Max SL	ML	CF	Iterations/Generations	Time (seconds)	Current Norm
Initial	-8.739	11.700	32.0000	0.3656	-	-	5.6569
GDA	-26.09	4.8416	97.5911	0.0496	489511	1500	31.5695
MA	-17.66	81.4113	621.6851	0.1310	583687	1500	160.574
GA	-14.59	7.1117	38.1390	0.1865	415024	1500	10.0104

b. Unbounded Currents – Minimum CF Target

	Max SL (dB)	Max SL	ML	CF	Iterations/Generations	Time (seconds)	Current Norm
Initial	-8.739	11.7000	32.0000	0.3656	-	-	5.6569
GDA	-14.16	11.3380	57.8711	0.2000	1484	0.2323	17.8862
MA	-13.99	324.7073	1625.73	0.2000	260226	212.159	462.584
GA	-13.98	10.8276	54.1504	0.2000	7417	18.9389	14.5170

c. Bounded Currents – Time Limit

	Max SL (dB)	Max SL	ML	CF	Iterations/Generations	Time (seconds)	Current Norm
Initial	-8.739	11.7000	32.0000	0.3656	-	-	5.6569
GDA	-22.55	5.6250	75.4526	0.0746	476416	1500	21.3683
MA	-23.80	4.3734	67.7721	0.0645	536105	1500	22.9587
GA	-9.381	14.3985	42.4016	0.3396	401151	1500	14.8178

d. Bounded Currents – Minimum CF Target

	Max SL (dB)	Max SL	ML	CF	Iterations/Generations	Time (seconds)	Current Norm
Initial	-8.739	11.7000	32.0000	0.3656	-	-	5.6569
GDA	-13.99	13.4762	67.4295	0.2000	13156	2.7931	17.4624
MA	-14.02	18.6197	93.4825	0.2000	14278	1.4964	22.7089
GA	-10.53	7.8978	26.7468	0.2953*	848912	3600	9.3934

*The target CF was not reached in this case

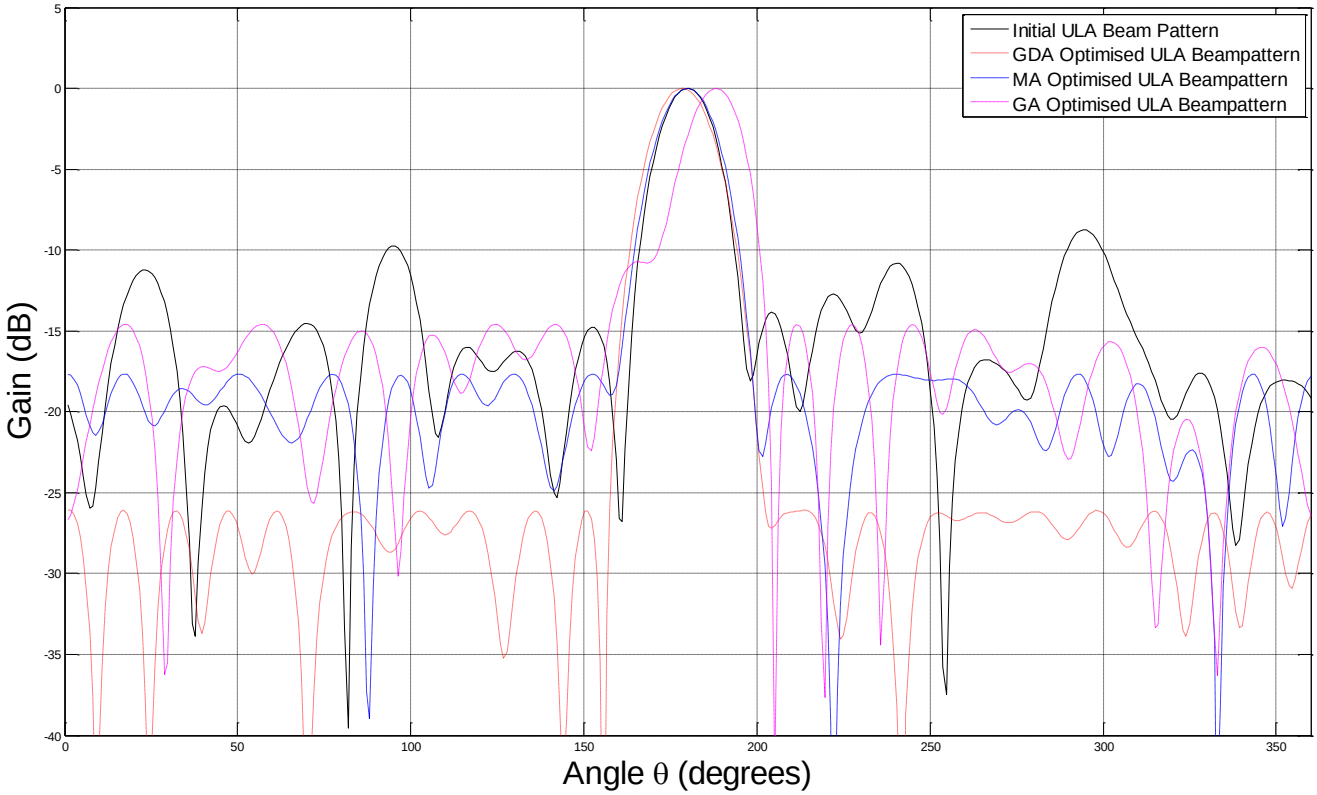

Figure 4.3.1 A plot comparing the initial and optimised beam patterns for WSN array in the timed-unbounded experiments.

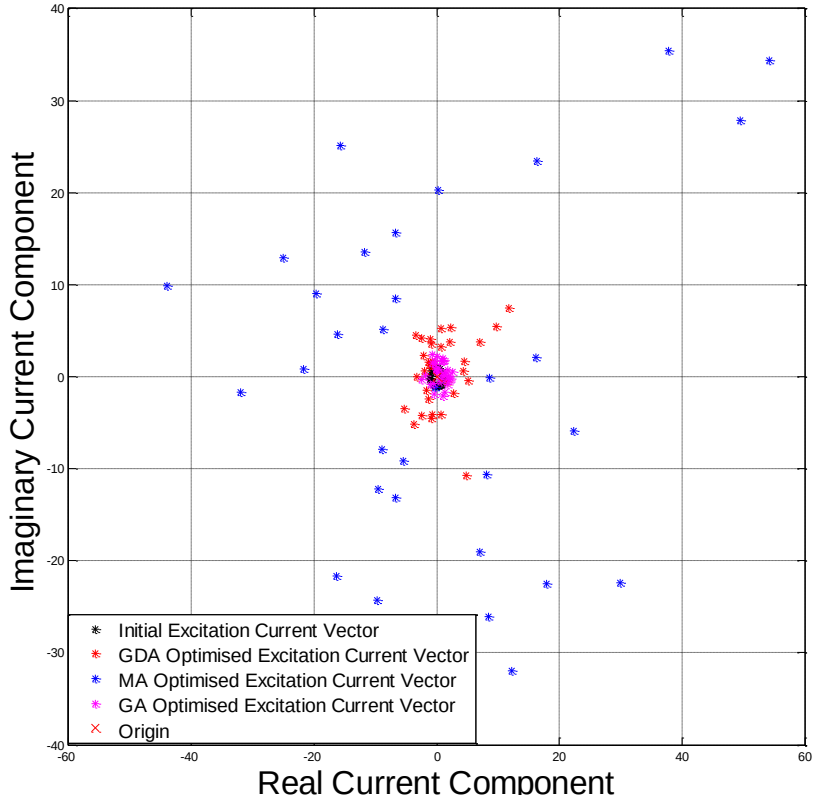

Figure 4.3.2 A scatter plot comparing the initial and optimised excitation current WSN array in the timed-unbounded experiments.

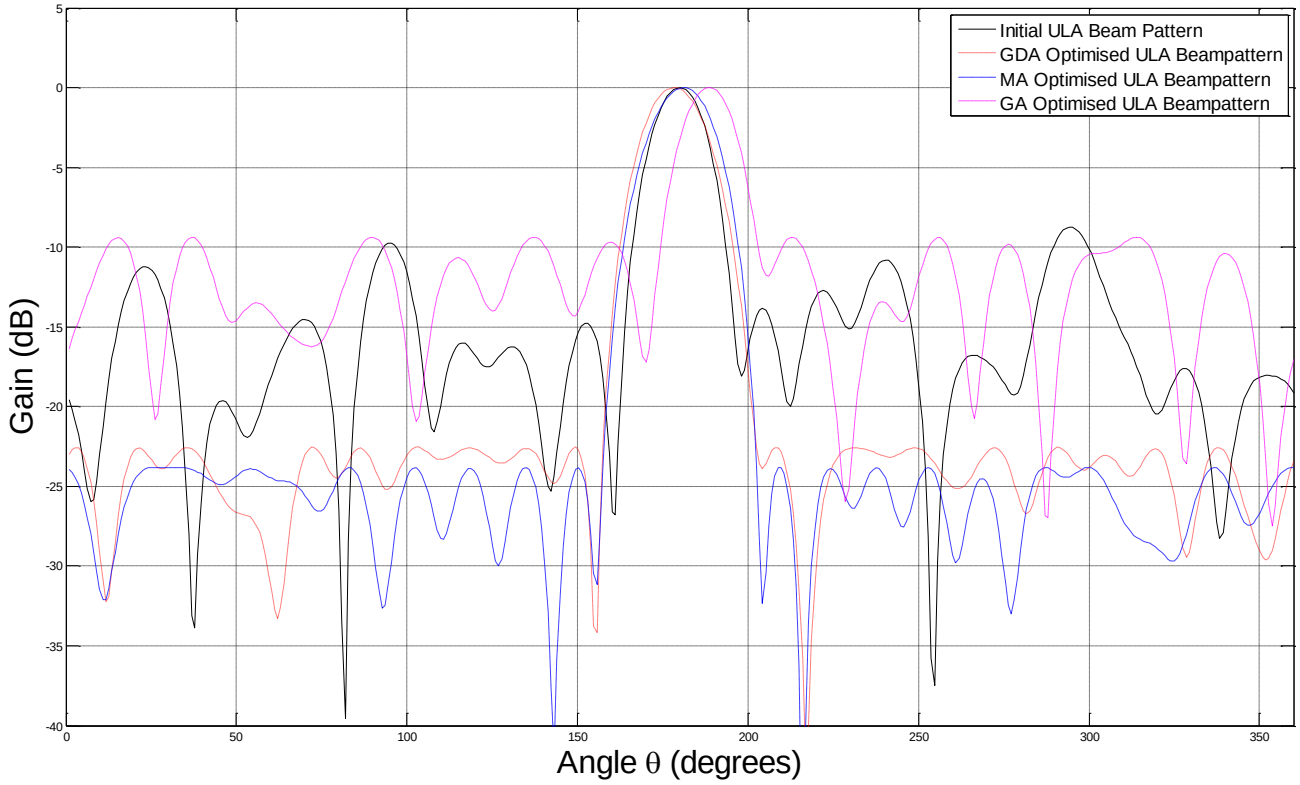

Figure 4.3.3 A plot comparing the initial and optimised beam patterns for WSN array in the time-bounded experiments.

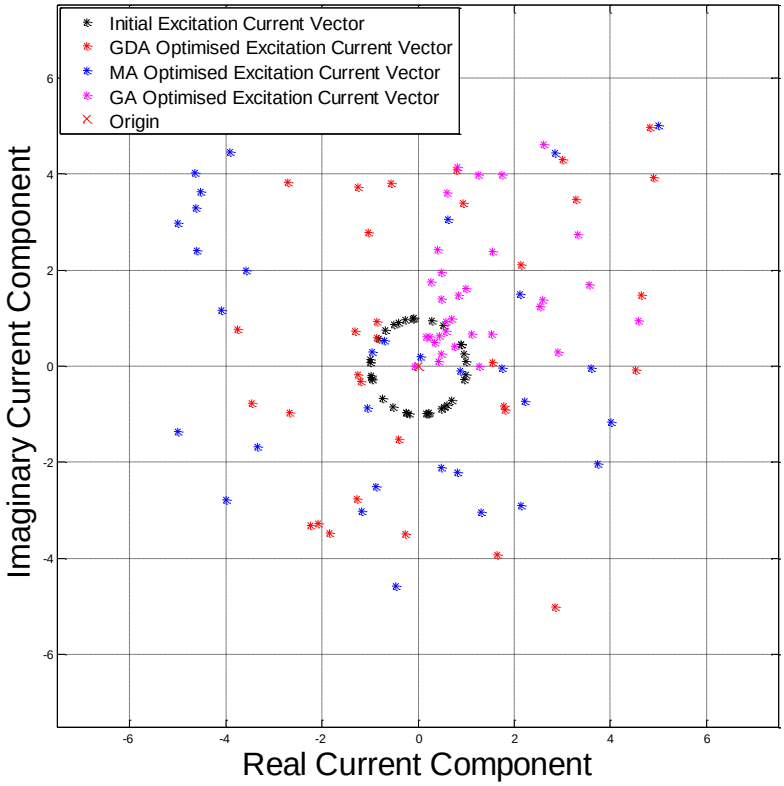

Figure 4.3.4 A scatter plot comparing the initial and optimised excitation current WSN array in the the time-bounded experiments.

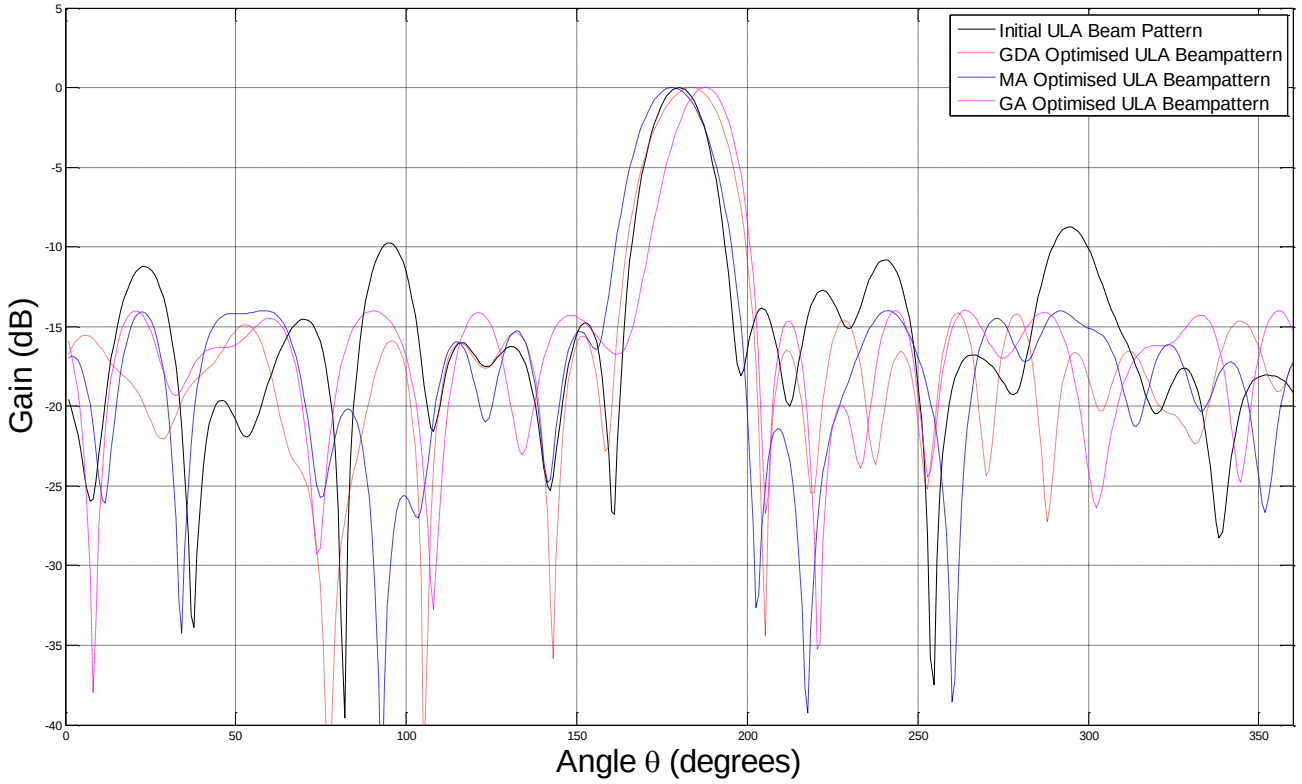

Figure 4.3.5 A plot comparing the initial and optimised beam patterns for WSN array in the minimum target CF-unbounded experiments.

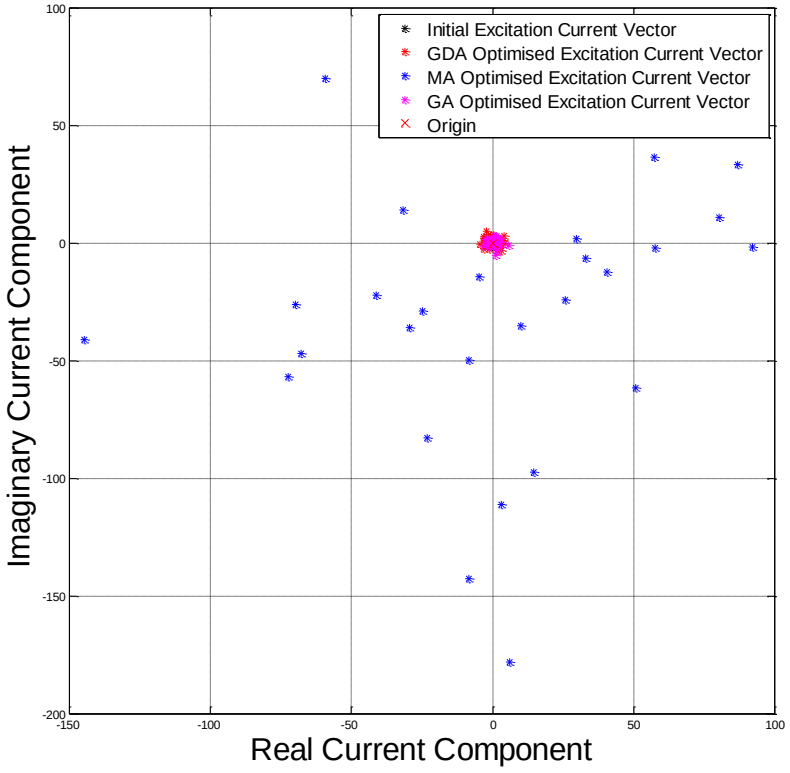

Figure 4.3.6 A scatter plot comparing the initial and optimised excitation current WSN array in the the minimum target CF-unbounded experiments.

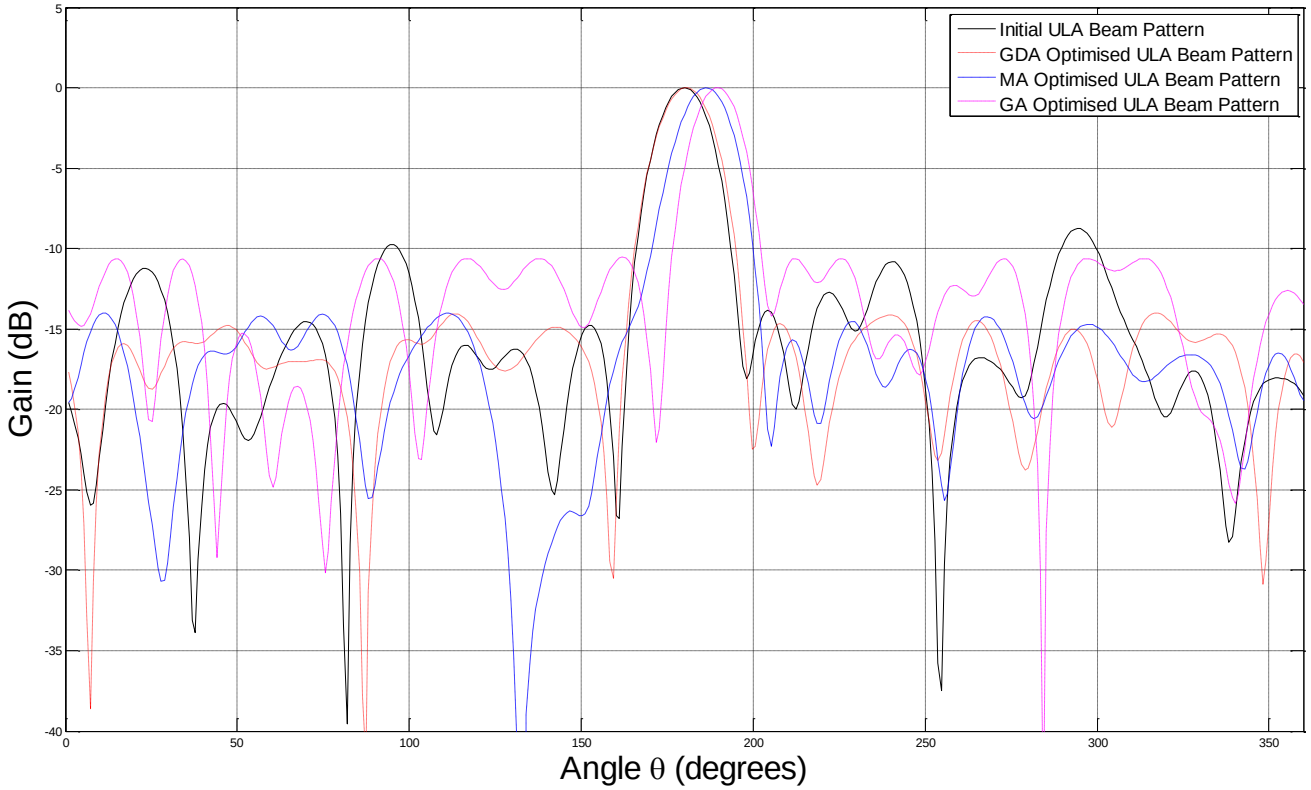

Figure 4.3.7 A plot comparing the initial and optimised beam patterns for WSN array in the minimum target CF-bounded experiments.

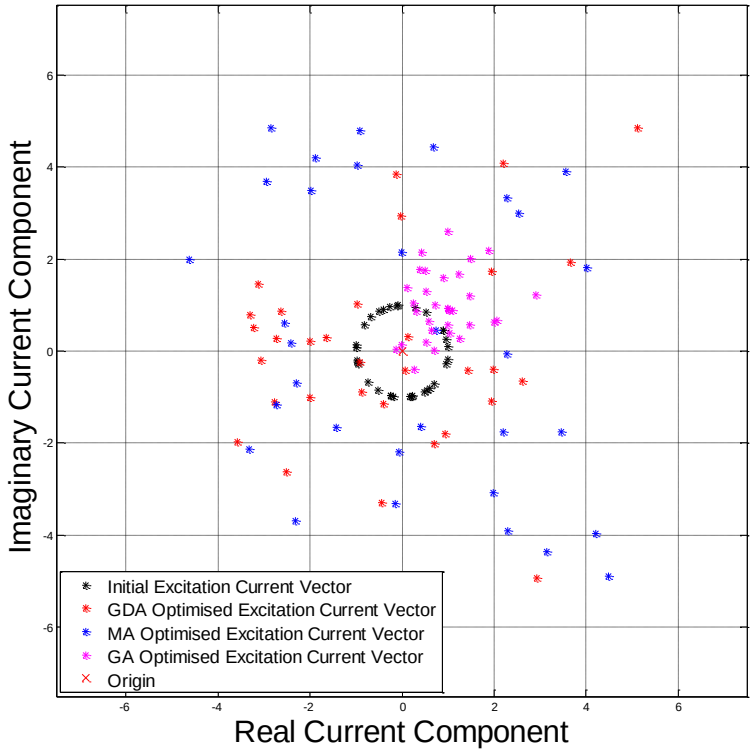

Figure 4.3.8 A scatter plot comparing the initial and optimised excitation current WSN array in the minimum target CF-bounded experiments.

Chapter 5

Discussion & Conclusion

In this chapter, the thesis is concluded and the results obtained are critically discussed following the experiments detailed in Chapter 5. The suitability of the chosen algorithms to the problem of beam pattern synthesis in sensor arrays is considered, as well as the limitations associated with the algorithms. Following this, future work which would aim to improve on the obtained results is presented, as well as speculative real-world applications of the optimisation algorithms.

5.1 Discussion of Results

The results detailed in Chapter 4 were significant as they indicated that metaheuristic and heuristic algorithms provide a capable method of reducing the max SL of a beam pattern produced by a sensor array using time or performance based stopping criteria. In the case of the ULA, it is thought that a near-optimum solution was approached when a reduction in the

maximum SL is chosen as the minimisation criteria. Following this, it was seen that the ULA with inactive element required additional computational effort by the algorithms as a result of its non-uniform geometry. In these two test cases, the results of the timed experiments provided similar CF values by each of the three algorithms. However, this was not the case with the minimum target CF experiments. The GA and MA were found to take up to 10 times as long in the bounded current experiments when compared with the equivalent times for the GDA. Nevertheless, the poor performance of the MA may be attributed to the relatively large excitation current vector produced. This is suggested by the fact that the MA was capable of quickly producing the target CF when its currents were bounded. Thus, as a result of the natural tendency of the MA is to increase its current values, bounded currents are required in order for algorithm to produce both improved and realistic results.

The final test case provided the sternest test to the optimisation algorithms and this is undoubtedly seen in the results provided in Chapter 5. The maximum SL values are seen to fluctuate significantly between each of the three algorithms, but it is found that the MA and GDA are the most successful in suppressing the maximum SL. Again, it was seen that the unbounded case sees the MA increase currents to an unrealistic level; however this is corrected in the bounded case where the MA eventually outperforms the GDA. The times provided by the GDA and MA in reaching the target CF value are noteworthy and suggest that the algorithms are capable of quickly adapting to changes in the positions of sensors a WSN array. Conversely, the results showed that the GA provided poorer results in the WSN array test case, when compared with the GDA and MA. The GA was also found to be the only algorithm that was incapable of reaching the minimum target CF in the bounded experiment. Thus it may be

concluded that the GA, in this implementation at the very least, is not capable of providing an optimised beam pattern when compared with the other algorithms tested. Thus it is clearly seen that the GA is limited with respect to the more complex beam pattern synthesis cases.

The seemingly slow nature of the GA may be categorised by repeated fitness function evaluations, as well as complex matrix manipulations when compared with the relative simplicity of the MA and GDA. Furthermore, it has been suggested that GAs suffer from the inability to know when to sacrifice short term-fitness in order to gain longer term fitness (Oonsivilai & Oonsivilai, 2009). This may be the case in this optimisation problem, such that the GA converges quickly to a local minimum in more complex cases, and therefore rapidly decreases the size of the search space. Furthermore, the stochastic nature of the GA may have negatively affected the samples provided for the results, such that an adequate solution was simply not found.

It is appropriate, when taking a high-level view of the results, to deduce that the MA and GDA performed equally well in the three test cases. In terms of optimisation time, the MA and GDA performed well in achieving a desired target CF, outperforming one another in different experiments. It was also consistently shown that the MA tended to increase the size of the currents feeding the sensor elements in an attempt to reduce the CF. The results showed that the resulting CF was similar to that which was provided by the GDA, however the large current norm ensures that the excitation current vector may not be implementable in practice. This problem was overcome in the bounded experiment which saw the MA and GDA results equalling each other in terms of time and performance measures.

Nevertheless, it should be stated that the high quality results provided by the GDA are somewhat unexpected. The GDA is, by its very nature, highly dependent on initial parameters and is characterised by, generally, producing a locally optimum solution. In spite of this, it appears that the introduction of the σ variable used to control the magnitude of the perturbations added to the excitation current vector allowed for the algorithm to traverse a wider search space and promoted slower convergence. Furthermore, it should be noted that the initial excitation current vector applied to the GDA may have benefited from the optimisation process as it allowed the GDA to quickly find a low CF value. Similarly, the MA may have benefited from the initial conditions, but if this was the case, the MA would have been capability of exploring the surrounding search area.

5.2 Conclusion

The work described in this thesis has been concerned with the development and application of optimisation algorithms for beam pattern synthesis in sensor arrays in an attempt to reduce the maximum SL of the beam pattern. Consulting relevant literature was indicative that the application of heuristics and metaheuristics to regular geometries was frequent, and thus a gap surrounding their application to more complicated geometries existed. A number of models of varying complexity were created and presented, as well as a suite of diverse optimisation algorithms. Considering the limitations of the algorithms presented, as well as all assumptions made, the results of the experiments have proven successful. The initial beam patterns were capable of being optimised with bounded, unbounded currents, and using a number of time and performance based criteria. Thus the metaheuristic and heuristic algorithms presented

have shown that they are a suitably flexible technique for beam pattern optimisation. The optimisation of a randomly distributed 2D WSN array was the first documented case in literature, and may prove effective in reducing the transmission energy overhead that is required in line with the increased utilisation of WSNs as part of IoT.

5.3 Future Work

The expected growth of WSNs as part of the IoT introduces a number of large and small scale phases which constitute possible future work in regards to this thesis. Logically speaking, the natural next step would be an expansion of the work outlined in this thesis. This would include the creation of a reannealing schedule in order to transform the MA towards a SA. The CF developed would also be improved, such that it would take more features of the beam pattern into account. The construction of an improved CF may prove useful in providing a lower maximum SL, specifically in the application of the GA which performed the poorest of the tested algorithms. The complexity of the 2D WSN array case could also be increased by introducing elements which are dynamic in 2D space. It would then be possible to measure each of the algorithm's abilities in adapting to changes in elements positions.

A number of more complicated topologies would also be investigated. Regular geometries such as the UCA and UPA would be ideal as a result of the numerous optimisation comparisons existing in literature. However, the optimisation of a beam pattern produced by a sensor array where the array elements are located in a 3D space would be highly beneficial to the field. The 3D case would, quite possibly, represent the most advanced IoT inspired topology possible as a

result of sensors which may be located in different dimensions. Finally, the addition of dynamic elements to the 3D WSN array model would add a further degree of complexity.

Additional algorithms, both heuristic and classical numerical methods, could also be implemented for comparison purposes. Optimisation algorithms which could be applied to the test cases outlined in this thesis include Particle Swarm Optimisation (PSO) and Tabu Search (TS). Although PSO and TS are metaheuristics, they differ from GA and MA in a number of ways, which makes them ideal with regards to their application to beam pattern synthesis problems. PSO is often compared with GA, but it offers a number of distinct differences in its computation (Hassan, et al., 2004). It has been claimed that PSO, which is similar to GA, can offer better results at a fraction of the computational complexity required in the GA. Thus, PSO may be more suitable to the problems outlined. Similarly in the case of TS, which is often likened to SA and MA, it offers a different dynamic by introducing memory structures. The memory structures describe solutions which have been visited previously by marking them as 'tabu'. Thus, the search space can be reduced in an attempt to find an optimum solution.

Finally, a major step with regards to future work would be the application of the algorithms a number of real world applications and scenarios. Although energy reduction was the aim of the optimisation process, the CF can be tailored in order to promote other beam pattern characteristics. Examples of this include decreasing the BW in order to aid security in or increasing the ML for increasing transmission distances. The techniques are therefore applicable in any scenario in which sensor nodes are capable of collaborating.

A variety of scenarios are presented in literature which would be majorly improved with the use of the methods outlined in thus thesis. In the past WSNs have been proposed with regards to monitoring the ocean environment. However, WSNs used to monitor ocean characteristics such as pollution, salinity, and temperature must reduce the power used in transmission where possible. This is as a result of the sensor nodes being equipped with a small battery, and due to high power consumption as a result of the poor underwater propagation characteristics, as well as the movement of the sensors with ocean currents (Reichenbach, et al., 2014). Other plausible applications include the use of WSNs in Deep Space Communications (DSC). Often in DSC, a probe or spacecraft which may contain a WSN is launched knowing that it will not return to earth. Therefore, flexible techniques are required in order to circumvent problems such as sensor element losses which may inherently occur on board, as well as reducing power consumption (Edgar & Callaway, 2003). The optimisation algorithms outlined in this thesis therefore offer a method for optimising the damaged beam pattern. However, these are two of many scenarios to which the methods outlined in this thesis could be applied. In theory, the application of optimisation algorithms can be applied in any scenario which constitutes numerous sensor elements that are capable of collaborating.

III. References

Ahmed, M. F. A. & Vorobyov, S. A., 2009. *Node selection for sidelobe control in collaborative beamforming for wireless sensor networks.* Perugia, Signal Processing Advances in Wireless Communications, 2009. SPAWC '09. IEEE 10th Workshop on, pp. 519-523.

Alcaraz, C., Najera, P., Lopez, J. & Roman, R., 2010. *Wireless Sensor Networks and the Internet of Things: Do We Need a Complete Integration?.* Tokyo, 1st International Workshop on the Security of the Internet of Things (SecIoT'10), IEEE.

Ares, F. et al., 1996. Synthesis of antenna patterns of circular arc arrays. *Electronics Letters,* 32(20), pp. 1845-1846.

Ares-Pena, F., Rodriguez-Gonzalez, J., Villanueva-Lopez, E. & Rengarajan, S., 1999. "Genetic algorithms in the design and optimization of antenna array patterns. *Antennas and Propagation, IEEE Transactions on,* 47(3), pp. 506-510.

Cardone, G., Cincotti, G. & Pappalardo, M., 2002. Design of wide-band arrays for low side-lobe level beam patterns by simulated annealing. *Ultrasonics, Ferroelectrics, and Frequency Control, IEEE Transactions on,* 49(8), pp. 1050-1059.

Chen, Y.-P. & Chen, Y.-Z., 2010. *A novel energy efficient routing algorithm for wireless sensor network.* Qingdao, Machine Learning and Cybernetics (ICMLC), 2010 International Conference on, pp. 1031-1036.

Chong, C.-Y. & Kumar, S. P., 2003. Sensor Networks: Evolution, Opportunities, and Challenges. *Proceedings of the IEEE,* August, 91(8), pp. 1247 - 1256.

Christin, D., Reinhardt, A., Mogre, P. S. & Steinmetz, R., 2009. *Wireless Sensor Networks and the Internet of Things: Selected Challenges.* Darmstadt, Proceedings of the 8th GI/ITG KuVS Fachgespräch Drahtlose Sensornetze, pp. 31-34.

Curletto, S. & Trucco, A., 2002. *Main lobe shaping in wide-band arrays.* Genova, OCEANS 2003. Proceedings.

De Jong, K., 1975. *An Analysis of the Behavior of a Class of Genetic Adaptive Systems.* First ed. Michigan: University of Michigan.

Desai, S. & Brooker, G., 2008. *Pattern synthesis of planar arrays using genetic algorithms.* Baltimore, Radar, 2008 International Conference on.

Dolph, C., 1946. A Current Distribution for Broadside Arrays Which Optimizes the Relationship between Beam Width and Side-Lobe Level. *Proceedings of the IRE,* June, 34(6), pp. 335 - 348.

DuFort, E., 1989. Pattern synthesis based on adaptive array theory. *Antennas and Propagation, IEEE Transactions on ,* 37(8), pp. 1011 - 1018 .

Edgar, H. & Callaway, J., 2003. *Wireless Sensor Networks Architectures and Protocols.* 1st ed. Florida: CRC Press.

Evans, D., 2011. *The Internet of Things: How the Next Evolution of the Internet Is Changing Everything,* San Jose: Cisco Systems, Inc..

Farhat, N. & Bai, B., 1987. Phased-array antenna pattern synthesis by simulated annealing. *Phased-array antenna pattern synthesis by simulated annealing,* 75(6), pp. 842-844.

Feng, J., Lu, Y.-H., Jung, B. & Peroulis, D., 2009. Energy Efficient Collaborative Beamforming in Wireless Sensor Networks. *Circuits and Systems. ISCAS 2009. IEEE International Symposium on,* 1(1), pp. 24-27.

Feng, J. et al., 2010. *Analysis of Energy Consumption on Data Sharing in Beamforming for Wireless Sensor Networks,* West Lafayette: Sch. of Electr. & Comput. Eng., Purdue Univ., West Lafayette.

Ferreira, J. & Ares, F., 1997. Pattern synthesis of conformal arrays by the simulated annealing technique. *Electronics Letters ,* 33(14), pp. 1187-1189.

Han, Z. & Poor, H., 2007. *Lifetime Improvement of Wireless Sensor Networks by Collaborative Beamforming and Cooperative Transmission.* Glasgow, IEEE Communications Society, pp. 3954 - 3958.

Hassan, R., Cohanim, B. & De Weck, O., 2004. *A Comparison of Particle Swarm Optimisation and the Genetic Algorithm,* Colorado: American Institute of Aeronautics and Astronautics.

Johnson, J. M. & Rahmat-Samii, Y., 1994. Genetic Algorithm and its Application in Antenna Design. *Genetic Algorithm and its Application in Antenna Design,* 1(1), pp. 326-329.

Khodier, M., 2013. Optimisation of Antenna Arrays using the Cuckoo Search Algorithm. *IET Microwaves, Antennas and Propogation,* 7(6), pp. 458-464.

Kumar, S., Priyesh, Singh, H. & Jha, R., 2009. *Radiation pattern of spherical phased antenna array with Dolph-Chebyshev's aperture distribution.* Bangalore, NAL-CSIR Council of Sci. & Ind. Res, pp. 1 - 4.

Lakshmi, V. R. & Raju, G. S. N., 2011. Pattern Synthesis using Genetic Algorithm for Low Sidelobe Levels. *International Journal of Computer Applications,* 31(4), pp. 53 - 57.

Lau, B. & Leung, Y., 2000. *A Dolph-Chebyshev approach to the synthesis of array patterns for uniform circular arrays.* Geneva, Circuits and Systems, 2000. Proceedings. ISCAS 2000 Geneva. The 2000 IEEE International Symposium on, pp. 124 - 127.

Li, M., McGuire, M., Ho, K. S. & Hayward, G., 2010. *Array element failure correction for robust ultrasound beamforming and imaging.* San Diego, Ultrasonics Symposium (IUS), 2010 IEEE .

Lin, C. & Yaan Li, 2010. *The method research of beamforming with array-element failure.* Changchun, Computer, Mechatronics, Control and Electronic Engineering (CMCE), 2010 International Conference on .

Mansuripur, M. & Tsai, D., 2011. *New Perspective on the Reciprocity Theorem of Classical Electrodynamics,* Tucson: College of Optical Sciences, The University of Arizona.

MathWorks, 2015. *Documentation - Global Optimisation toolbox.* [Online]
Available at: http://uk.mathworks.com/help/gads/index.html
[Accessed 2015 03 19].

Metropolis, N. et al., 1943. Equation of State Calculations by Fast Computing Machines. *The Journal of Chemical Physics,* 21(6), pp. 1087-1092.

Mudumbai, R., Barriac, G. & Madhow, U., 2007. On the Feasibility of Distributed Beamforming in Wireless Networks. *Wireless Communications, IEEE Transactions on*, 21 May, 6(5), pp. 1754 - 1763.

Murino, V., 1995. *Simulated Annealing Approach for the Design of Unequally Spaced Arrays.* Detroit, Acoustics, Speech, and Signal Processing, 1995. ICASSP-95., pp. 3627-3630.

Murino, V., Trucco, A. & Regazzoni, C., 1996. Synthesis of unequally spaced arrays by simulated annealing. *Signal Processing, IEEE Transactions on,* 44(1), pp. 119-122.

Ochiai, H., Mitran, P., Poor, H. V. & Tarokh, V., 2004. *Collaborative Beamforming in Ad Hoc Networks.* San Antonio, Information Theory Workshop. IEEE, pp. 396 - 401.

Oonsivilai, A. & Oonsivilai, R., 2009. *A Genetic Algorithms Programming Application in Natural Cheese Products,* Nakhon Ratchasima: Suranaree University of Technology.

Peters, T., 1989. *Application of a conjugate gradient method to the synthesis of planar arrays.* San Jose, Antennas and Propagation Society International Symposium, pp. 304- 307.

Rathod, M. & Meera, A., 2014. A Review on Antenna Radiation Pattern Synthesis. *IOSR Journal of Electronics and Communication Engineering (IOSR-JECE),* 9(5), pp. 01-03.

Reichenbach, F., Handy, M. & Timmermann, D., 2014. *Monitoring the Ocean Environment with Large-Area Wireless Sensor Networks,* Rostock: Institute of Applied Microelectronics and Computer Science, University of Rostock.

Rutenbar, R., 1989. Simulated annealing algorithms: an overview. *Circuits and Devices Magazine, IEEE,* 5(1), pp. 19-26.

Shebli, F., Dayoub, I., Rouvaen, J. M. & Zaouche, A., 2007. *A New Optimisation Approach for Energy Consumption Within Wireless Sensor Networks.* Washington, IEEE Computer Society, pp. 13-19.

Skolnik, M., Nemhauser, G. & Sherman, J. I., 1964. Dynamic programming applied to unequally spaced arrays. *Antennas and Propagation, IEEE Transactions on ,* 12(1), pp. 35-43.

Taskin, A. & Gurel, C. S., 2003. *"Antenna Array Pattern Optimisation In The Case Of Array Element Failure.* Munich, Microwave Conference, 2003. 33rd European.

Tokunaga, S. et al., 2008. *Power saving effect of sensor collaborative beamforming for wireless ubiquitous network systems.* Tokyo, Communications, 2008. APCC 2008. 14th Asia-Pacific Conference on, pp. 1-5.

Vasseur, J.-P. & Dunkels, A., 2010. *Interconnecting Smart Objects with IP - The Next Internet.* 1 ed. .: Morgan Kaufmann.

Vu, C. T., 2009. *Distributed Energy Efficient Solutions for Area Coverage Problems in Wireless Sensor Networks,* Georgia: College of Arts and Sciences, Georgia State University.

Wong, C. H. et al., 2012. *Node collaboration for distributed beamforming in wireless sensor networks.* Penang, Control System, Computing and Engineering (ICCSCE), 2012 IEEE International Conference on.

Yanli, Y. & Yingmin, W., 2010. *Beam Pattern Optimisation Using MVDR and Simulated Annealing.* Nanjing, Service Oriented System Engineering (SOSE), 2010 Fifth IEEE International Symposium on , pp. 117 - 120.

Zhou, P., Ingram, M. & Anderson, P., 1998. *Synthesis of minimax sidelobes for arbitrary arrays.* Georgia, Sch. of Electr. & Comput. Eng., Georgia Inst. of Technol., pp. 1759 - 1760.